International Journal of Biological Macromolecules 353 (2026) 151192

Contents lists available at ScienceDirect

International Journal of Biological Macromolecules

journal homepage: www.elsevier.com/locate/ijbiomac

Natural deep eutectic solvent-assisted incorporation of anthocyanins into cellulose acetate nanofibers for halochromic sensors

Mirella Romanelli Vicente Bertolo-Cagnoto [a,b,*], Augusto Duarte Alvarenga [a,c], Laís Angelice de Camargo [a], Kelcilene Bruna Teodoro Costa [a], Daniel Souza Correa [a,**]

[a] Nanotechnology National Laboratory for Agriculture (LNNA), Embrapa Instrumentation, Sao Carlos, SP, Brazil
[b] University of Sao Paulo (USP), Luiz de Queiroz College of Agriculture (ESALQ), Department of Food Science and Technology (LCA), Piracicaba, SP, Brazil
[c] University of Sao Paulo (USP), Sao Carlos Institute of Chemistry (IQSC), Sao Carlos, SP, Brazil

ARTICLE INFO

Keywords:
Cellulose acetate
Intelligent materials
Anthocyanins
Chemical sensor
Functional nanofibers
Food spoilage
Food security
Food safety
Food sensor
Colorimetric sensor

ABSTRACT

Intelligent food packaging can help reduce food waste by providing consumers real-time information about product freshness. They can be produced using natural pigments with pH-dependent color changes, which makes them promising candidates for colorimetric sensors. This study reports the development, through solution blow spinning (SBS), of cellulose acetate (CA)-based nanofibers loaded with anthocyanins solubilized in natural deep eutectic solvents (NADES). CA nanofibers were obtained by SBS using CA/PEO (polyethylene oxide) co-solutions, followed by PEO removal. Anthocyanins from grape pomace (GP), sweet potato (SP), and black carrot (BC) were incorporated into pectin solutions solubilized in a choline chloride–glycerol NADES (CC-GLY), which were then used to modify the fibrous membranes by immersion, yielding halochromic sensors. These sensors were characterized regarding their morphological, thermal, and water-related properties. Anthocyanins incorporation decreased CA onset degradation temperatures and increased its melting enthalpy, suggesting improved chain packing. The fibers containing anthocyanins were more hydrophilic and more soluble. Exposure to ammonia vapor produced visible colorimetric responses, with CA/BC achieving the highest ΔE values (24.60 ± 0.50) and a detection limit as low as 1.73×10^{-6} mol L^{-1}. Finally, a proof-of-concept assay confirmed CA/BC applicability for monitoring fish (salmon) spoilage via headspace exposure (ΔE = 26.52 ± 0.97 after 144 h at 4 °C and ΔE = 28.49 ± 1.04 after 48 h at 25 °C). The results demonstrate that CA nanofibers doped with anthocyanins are promising natural materials for intelligent packaging applications, enabling rapid and sensitive detection of food spoilage.

1. Introduction

The development of innovative and functional materials is of outmost importance to help prevent food waste and food loss, a serious global problem and one of the biggest challenges of the UN 2030 agenda [1]. The so-called intelligent food packaging stands out among these functional materials, aiming to inform the consumer, at the time of purchase or pre-consumption, the real freshness of the packaged food and whether it is still suitable for consumption [2]. The development of intelligent packaging materials usually involves the use of tags or devices, which may present numerous functions, acting as pH, time/temperature or ripeness indicators, biosensors, among others [3,4].

Halochromic pH indicators are colorimetric devices that change color rapidly when the pH of the food or the environment in which it is contained is modified [5]. These pH changes are common in food matrices, due to the occurrence of various deteriorative reactions that alter the composition of the food, leading to the production of acidic or basic compounds [2,6]. Protein-rich foods, such as fish and meat, for example, undergo decarboxylation of their amino acids, producing volatile nitrogen compounds, like ammonia and biogenic amines [7]. The accumulation of such compounds leads to changes in the pH of the food and in its sensory perception and can result in its rejection by consumers [8].

Anthocyanins are molecules classified as flavonoids, whose

* Correspondence to: M.R.V. Bertolo-Cagnoto, University of Sao Paulo (USP), Luiz de Queiroz College of Agriculture (ESALQ), Department of Food Science and Technology (LCA), Piracicaba, SP, Brazil.
** Corresponding author.
E-mail addresses: mirella.bertolo@usp.br (M.R.V. Bertolo-Cagnoto), daniel.correa@embrapa.br (D.S. Correa).

https://doi.org/10.1016/j.ijbiomac.2026.151192
Received 16 December 2025; Received in revised form 13 February 2026; Accepted 28 February 2026
Available online 4 March 2026

structures are pH-dependent and have distinct colors, being interchangeable and favored according to the pH of the medium [5]. The color changes of anthocyanins can be generalized as going from red in an acidic medium (predominant structure of the flavylium cation) to yellow in a basic medium (predominant structure of chalcones) [9]. Among the main natural sources of anthocyanins, one can mention grapes pomace [10], black [11], and purple sweet potatoes [12].

Anthocyanins can be incorporated into a wide variety of materials in terms of composition and shape, with emphasis in polymeric nanofibers obtained by solution blow spinning (SBS). These fibers are advantageous compared to other materials due to their high surface area/volume ratio, high porosity, ability to encapsulate compounds, and to gradual release them when necessary [5]. In recent years, SBS has emerged as a compelling alternative to traditional fiber fabrication methods such as electrospinning (ES) for the preparation of functional materials, including those tailored for halochromic sensing applications. Unlike ES, which relies on high-voltage electric fields and strict solution conductivity requirements, SBS uses a pressurized gas stream to draw polymer solutions into ultrafine fibers, eliminating the need for high-voltage setups and expanding the compatibility with a wider range of solvents and sensitive chromogenic agents [13]. This approach enables higher production rates and lower operational costs, facilitating the rapid and scalable fabrication of nanofibrous mats with high specific surface area and porosity, characteristics that are particularly beneficial for enhancing the sensitivity and response time of halochromic sensors [13,14].

One of the key requirements to produce nanofibers aimed at food packaging is the selection of suitable polymers, which should preferably be renewable, eco-friendly, and non-toxic [1,5]. Cellulose acetate (CA) is one of the most important cellulose derivatives; its desirable characteristics, such as fiber-forming properties and biodegradability, make it suitable for food packaging, either as a base packaging material or as a colorimetric device [15]. Zhang et al. (2022) [5], for instance, produced colorimetric CA-based membranes incorporated with *Perilla frutescens* (L.) Britt. anthocyanins and chamomile essential oil by electrospinning; Freitas et al. (2020) [2], in turn, used CA to develop intelligent films containing red cabbage extract.

Another emerging hotspot in the development of intelligent food packaging is the application of natural deep eutectic solvents (NADES). These solvents are formed by mixtures of natural compounds, mainly primary metabolites, which generate eutectic liquids characterized by high extractive power, remarkable solvation capacity, good chemical stability, low volatility, and low toxicity [16]. Such solvents can be used in both the extraction and solubilization of anthocyanins, facilitating their incorporation into polymeric matrices or materials produced by SBS, due to the formation of hydrogen bonds between the NADES compounds, anthocyanins, and the polymers [17,18].

Although cellulose acetate–based halochromic sensors incorporating anthocyanins have been investigated before, most reported systems rely on solvent casting or ES approaches. For instance, Freitas et al. [2] developed CA films by solvent casting, while Zhang et al. [5] reported electrospun CA-anthocyanin nanofibrous mats with effective colorimetric responses. Recent nano- and microfibrous halochromic mats prepared by ES and related techniques further demonstrate the potential of fibrous architectures for sensing applications [19–21]. However, these approaches typically rely on conventional organic solvent systems and high-voltage processing, and their discussion is often focused on sensing performance rather than on process simplicity, scalability, or application-oriented fabrication considerations.

In this context, the present study introduces a pectin-NADES-assisted strategy to enable homogeneous incorporation of anthocyanins into CA nanofibrous mats produced by SBS. The use of NADES provides a versatile carrier phase that facilitates pigment solubilization, handling, and incorporation while avoiding additional organic solvents. Pectin further promotes pigment retention at the fiber surface through non-covalent interactions with anthocyanins, enabling post-spinning functionalization without interfering with fiber formation. In parallel, SBS allows the rapid fabrication of highly porous nanofibrous mats without high-voltage requirements, offering improved scalability and process robustness compared to ES [14]. Together, these aspects distinguish the proposed approach from previously reported CA-anthocyanin and electrospun systems and highlight its relevance for intelligent packaging applications.

Fig. 1 shows a schematic representation of the approach employed, including the CA-based nanofibers obtention by SBS (Fig. 1(A)), the incorporation of different anthocyanins (from grape pomace – GP, sweet potatoes – SP, and black carrots – BC) using NADES (Fig. 1(B)), the colorimetric evaluation of the developed materials (Fig. 1(C)), and their application in salmon packaging to evaluate food spoilage as a proof-of-concept (Fig. 1(D)). The results showed that the nanofibrous mats exhibited pH-sensitive color changes while maintaining morphological, physical-chemical, and thermal properties suitable for food applications, which offers valuable insights for the development of low-cost and eco-friendly solutions for intelligent packaging.

2. Materials and methods

2.1. Materials

The three anthocyanins used in this study were kindly provided by Oterra® (Hørsholm, Denmark). The base of ColorFruit® Bordeaux 104 WSP is grape pomace (GP), the base of FruitMax® Red 104 WSP is Hansen sweet potato (SP) and the base of ColorFruit® Red 108 WSP is black carrot (*Daucus Carota L.*) (BC). All the products are standardized on color strength in color units (CU) per kilogram, being: 11.5–12.5 CU/kg for GP, 7.0–9.0 CU/kg for SP, and 37–43 CU/kg for BC.

Cellulose acetate (CA, product number 419028, purity ≥97%, Mn = 50,000 g mol^{-1}, DS = 2.5), pectin from apple (product number 76282, purity ≥90%, Mr. = 30,000–100,000 g mol^{-1}, esterification degree = 70–75%, galacturonic acid residues ≥74%) polyethylene oxide (PEO, MW = 100,000 g mol^{-1}), acetone, chloroform, methanol, and *N*,*N*-dimethylformamide (DMF) were supplied by Sigma-Aldrich® (St. Louis, MO, USA). All reagents and solvents used in the preparations and characterizations (described in detail in the next sections) were of PA grade and used without further treatment.

2.2. Anthocyanins characterization

2.2.1. Total anthocyanins content (TAC)

The anthocyanins had their TAC determined according to the pH differential method [16,22]. For that, the pigments were solubilized in water and diluted 5-7× in two different buffers (pH 1.0 and pH 4.5). Their absorbances were then measured (after 30 min in the dark) at 520 and 700 nm. TAC (expressed as mg cyanidin 3-glucoside L^{-1}) was calculated according to Eq. (1) and converted to mg cyanidin 3-glucoside 100 g^{-1} dry matter (DM) according to the anthocyanin's solutions concentration.

$$TAC\ \left(mg\ cyanidin\ 3-glucoside\ L^{-1}\right) = \frac{A\ x\ MW \times DF \times 1000}{\varepsilon} \quad (1)$$

In the equation, $A = (Abs_{520nm} - Abs_{700nm})_{pH\ 1.0} - (Abs_{520nm} - Abs_{700nm})_{pH\ 4.5}$, *MW* is the molecular weight (449.2 g mol^{-1}) of cyanidin 3-glucoside, *DF* is the dilution factor, 1000 is the conversion factor from g to mg, and ε is the molar extinction coefficient of cyanidin-3-glucoside (26,900 L mol^{-1} cm^{-1}). The assay was performed in triplicate for each anthocyanin.

2.2.2. pH sensitivity

Initially, a NADES based on choline chloride and glycerol (both Sigma-Aldrich®) was prepared following the methodology described by Bertolo et al. (2025) [23]. The ratio between the components was 2:1, and 20% (*w*/w) of water was added to the system. The solvent, named

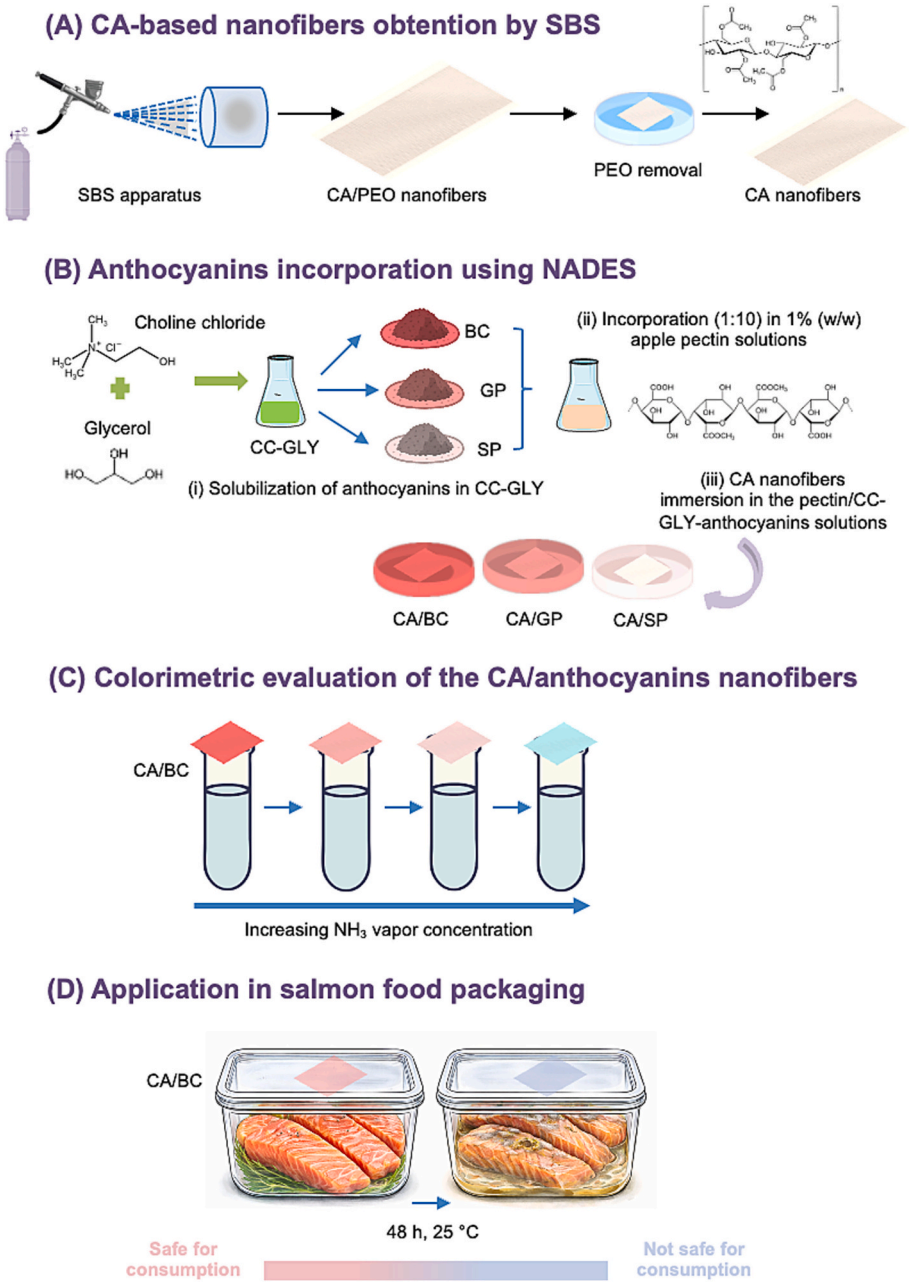

Fig. 1. (A) Production of cellulose acetate (CA) nanofibers by solution blow spinning (SBS), (B) use of a choline chloride-glycerol (CC-GLY) NADES for the solubilization of different anthocyanins and their incorporation into pectin solutions followed by CA-nanofibers immersion, (C) the colorimetric assays performed with the developed nanofibrous mats, and (D) their application as a proof-of-concept in salmon packaging to evaluate food spoilage.

CC-GLY, was used as a carrier for the anthocyanin's incorporation in the nanofibers, as it will be explained in section 2.4.

For the determination of the anthocyanin's sensitivity to pH variations, the three pigments were solubilized in CC-GLY, at 30 mg mL^{-1}, and the solutions were diluted 5× in pH 2–13 solutions, prepared by mixing a stock acetic acid solution (50 g L^{-1}) with a sodium hydroxide solution (2 mol L^{-1}) in different proportions, until the desired pH was reached (confirmed through the use of a calibrated pH meter). The visible spectra (UV-1900 spectrophotometer, Shimadzu, Kyoto, Japan) of the anthocyanins solutions were then recorded at 400–800 nm [24].

2.3. Nanofibers production and optimization by solution blow spinning

The CA nanofibers were prepared from the spinning of a mixture of equal volumes (1:1 ratio) of CA and PEO solutions. The CA solution was prepared by solubilizing the polymer at an optimized concentration of 15% *w/v* in an acetone/DMF solvent mixture (3:1, *v*/v) for 15 h. The PEO solution, on the other hand, was prepared by solubilizing PEO at 10% w/v in a mixture of chloroform/methanol (3:2, v/v) for 1 h.

After the preparation of the CA/PEO mixture, the nanofibers were fabricated using a solution blow spinning (SBS) system, which consisted of a syringe pump (model NE-300, Syringe Pump), a concentric needle setup, a pressurized gas source, and a rotating collector. The spinning parameters were optimized in subsidiary experiments and then set as: ejection rate of the solution of 20 mL h^{-1}, air pressure of 2 bar, working distance of 30 cm, collector rotation speed of 180 rpm, and ambient conditions of 20–30 °C and 40–60% relative humidity. The CA-PEO fibers were carefully washed twice to remove PEO, by immersion in 10 mL of deionized water for 10 min each. After washing and removing excess water, the fibers were dried in an oven at 50 °C for 18 h.

2.4. Nanofibers immersion in the anthocyanins solutions

Initially, a 1% (*w*/w) apple pectin solution was prepared in water, by solubilization at 60 °C for 30 min. After cooling down to room temperature, the solutions of anthocyanins in CC-GLY (detailed in section 2.2) were incorporated into the pectin solution, at a 1:10 ratio. Therefore, the final formulations (i.e., pectin + CC-GLY + anthocyanins) contained anthocyanins at a concentration of 3 mg mL^{-1}.

The CA nanofibrous mats were then cut into 10 × 5 cm^2 specimens and immersed into 10 mL of the final anthocyanins solutions, for 30 min. After draining, the nanofibrous mats were dried at room temperature for 24 h and stored in desiccators protected from light for the subsequent characterization and pH sensitivity analysis. For means of comparison, nanofibrous mats without anthocyanins (i.e., CA only) were also characterized by the assays described in the next section.

2.5. Nanofibers characterization

2.5.1. Scanning electron microscopy (SEM)

The morphology of the CA-based nanofibers was examined by scanning electron microscopy (SEM) using a JEOL® JSM-6701F microscope equipped with a field emission gun. A small portion of each sample was deposited onto a carbon tape and further coated with a thin gold layer (15 nm) using a sputter coater (Leica EM SCD050). The accelerating voltage applied to obtain the images was 10 kV. The average diameter of the nanofibers was determined using ImageJ® software (national Institute of Health, USA), with approximately 150 measurements.

2.5.2. Fourier transform infrared spectroscopy – Attenuated total reflectance (FTIR-ATR)

The functional groups of the CA-based nanofibrous mats were identified on a FTIR spectrometer Bruker Vertex 70 equipped with an attenuated total reflectance accessory (ATR) with diamond crystal. The spectra were collected from 4000 to 400 cm^{-1}, with a resolution of 4 cm^{-1} and 32 scans per sample.

2.5.3. Thermal properties

The thermal stability of the samples was characterized by thermogravimetry (TGA, model Q500, TA Instruments®, New Castle, Delaware, USA). Approximately 7–8 mg of the samples were used for the analysis. The experiments were carried out with a heating rate of 10 °C min^{-1} from 25 to 600 °C in synthetic air atmosphere with a flow rate of 60 mL min^{-1}.

The thermal events of the samples were evaluated by differential scanning calorimetry (DSC). The analyses were performed using a Q100 TA Instruments calorimetric analyzer. In order to investigate the interactions between CA and anthocyanins, the samples (5.0 ± 1.0 mg) were heated under an isothermal procedure (20 min at 150 °C) to erase thermal history without inducing degradation of CA [25]. After this, the samples were heated from 50 to 300 °C using a heating rate of 10 °C min^{-1} under nitrogen flow (60 mL min^{-1}). The thermograms related to the second heating of the samples were recorded and analyzed.

2.5.4. Water contact angle (WCA)

The sessile drop technique (Theta Lite optical tensiometer, dpUnion, Jabaquara, Brazil) was applied to evaluate the contact angle between water droplets (3 μL) and the surface of the nanofibrous mats, in order to investigate their wettability. Optical images were acquired at every 0.2 s after droplet fall using OneAttension® software. The test was performed at least 5 times for each mat, and the reported WCA was standardized across samples as the average of the angle reported in the second frame after the water droplet contacted the fiber surface.

2.5.5. Weight gain assessment

The incorporation of the pectin-NADES-anthocyanin system onto the cellulose acetate (CA) nanofibrous mats (1 cm^2) was quantitatively evaluated by determining the mass per unit area. For that, the mass of each sample was recorded and normalized by its surface area. Measurements were performed in triplicate for each mat.

2.5.6. Water-induced mass loss

The mass loss in water of the CA-based nanofibrous mats, with and without anthocyanins, was determined using the procedure described by Chentir et al. (2023) [26] with modifications. Briefly, specimens of approximately 2 cm^2 of each mat were dried at 40 °C for 24 h in an air circulation oven (Quimis, Diadema, Brazil) and their initial dry weight (W_1) was determined. Then, the specimens were immersed in 50 mL of distilled water, and placed in a shaker (TE421, Tecnal, Piracicaba, Brazil) at 76 rpm for 24 h, at 25 °C. After this period, the water was drained and the specimens were dried again at 40 °C for 24 h, in order to determine their final dry weight (W_2). Water-induced mass loss (%) was calculated according to Eq. (2). The assay was performed in triplicate for each mat.

$$\textit{Water induced mass loss}\ (\%) = \left(\frac{W_1 - W_2}{W_1}\right) \times 100 \tag{2}$$

2.6. pH sensitivity

2.6.1. pH responsiveness

The pH responsiveness of the CA-based nanofibrous mats containing the three anthocyanins was evaluated by immersing for 30 s rectangular pieces of the materials in solutions at pHs varying from 2 to 12 (prepared as described in section 2.2.2). Digital photographs of the mats were taken right after removal from the solutions, in a chamber with controlled luminosity (Puluz® Photo Light Box). The photographs were used for the determination of the color parameters (L* – lightness, a* - redness/greenness, and b* - yellowness/blueness values), with the Color Detector® app. The total color difference (ΔE) of the nanofibrous mats was calculated according to Eq. (3). In the equation, L^*, a^*, and b^* represent the color parameters of the fibers after the immersion in solutions of different pHs, and L_0^*, a_0^*, and b_0^* are their initial color parameters (i.e., before immersion).

$$\Delta E = \sqrt{\left(L^* - L_0^*\right)^2 + \left(a^* - a_0^*\right)^2 + \left(b^* - b_0^*\right)^2} \tag{3}$$

2.6.2. Colorimetric responses to volatile ammonia

To attest the color change of the anthocyanins-containing nanofibrous mats in basic media (corresponding to the pH range of the volatile nitrogen compounds released during food deterioration [27], their colorimetric response was first evaluated by exposing specimens (~4 cm^2) to the headspace of flasks containing distilled water (1 mL, as a control medium) and a concentrated ammonium hydroxide solution (30% *v*/v, 1 mL), 1 min each. Since the colorimetric response was too fast to be captured by a colorimeter, photos of the fibers were taken in a chamber with controlled luminosity, and the color difference between the samples was attested by treating the photos with the Color Detector® app [5]. The color parameters of the materials were determined and used for total color difference (ΔE) calculation.

The pH sensitivity of CA/BC, the mat with the best colorimetric response in the previous assay, was further analyzed by the construction of a curve of ΔE versus ammonium hydroxide concentration. For that, the same parameters of headspace exposure described before were followed, for different NH_4OH concentrations (from 0.001 to 0.2 mol L^{-1}). The exposure time for this assay was 5 min, to ensure that the color change occurred even at the lowest ammonia concentrations. With the aid of the calibration curve, the limits of detection and quantification (LOD and LOQ, respectively) were determined.

2.6.3. Proof-of-concept in real food packaging

A proof-of-concept assay was conducted to evaluate the performance

of the colorimetric sensor under real food packaging conditions. For this, fresh salmon samples were used as a model protein-rich food prone to the release of volatile basic nitrogen compounds during spoilage. Approximately 20 g of fresh raw salmon were placed into transparent, hermetically sealable containers. CA/BC mats (4 cm^2) were affixed to the upper region of the inner lateral wall of each container, avoiding direct contact with the food and allowing exclusive exposure to the package headspace.

Two storage conditions were evaluated: refrigeration at 4 °C and storage at room temperature (25 °C). For each condition, three independent containers were prepared. The containers were sealed immediately after sensor placement and salmon loading. Sensor color changes were monitored over time by photographic recording. Images were captured at 0, 2, 4, and 6 h, followed by 24 h, and subsequently every 24 h up to 144 h of storage. All photographs were taken under controlled and constant lighting conditions to minimize external variability. The color parameters of the fibrous mats were determined as described in the previous sections and used for total color difference (ΔE) calculation.

3. Results and discussion

3.1. Anthocyanins characterization

The anthocyanins selected for this study, derived from grape pomace, purple sweet potato, and black carrot, were chosen based on sustainability aspects, compositional diversity, and their suitability for halochromic sensing [10,11]. Grape pomace anthocyanins stand out as a value-added use of an abundant agro-industrial byproduct, contributing to waste reduction and circular economy strategies while offering a chemically diverse anthocyanin profile rich in malvidin-, delphinidin-, and cyanidin-based glycosides [9,10]. Purple sweet potato and black carrot anthocyanins, obtained from renewable plant sources widely used in the food industry, are recognized for their high stability and strong chromatic response, particularly due to their high degree of acylation [12,28]. The combined use of these three anthocyanin sources enables a comparative assessment of how differences in pigment content, molecular structure, and color strength influence pH responsiveness and colorimetric performance when these pigments are incorporated into CA-based materials [29,30].

The extracts used in this study were first characterized by their total anthocyanins content (TAC), which reflects the actual amount of anthocyanins extracted from the original source. The TAC values found by the pH differential method were 3.79 ± 0.54, 73.72 ± 0.36, and 60.03 ± 1.30 mg cyanidin 3-glucoside 100 g^{-1} DM, for SP, BC, and GP samples, respectively. The anthocyanins contents depend on several factors, such as the origin of the anthocyanins, the extraction methods, and sample preparation [31]. In general, black carrots present higher anthocyanin concentration (values up to 175 mg 100 g^{-1} DM) than grape pomace and sweet potato or other fruits and vegetables, which is also related to their stronger coloration [29,32].

Fig. S1 shows the color change and the UV–Vis spectra of the anthocyanins solutions at different pH values (from 2 to 13). All the anthocyanins used in this study were sensitive to changes in pH and showed colors ranging from pink (at more acidic pH) to green and yellow at more alkaline pH, suggesting they can be used as visual indicators of food deterioration in packaging materials [33]. Although all solutions were at the same concentration (6 mg mL^{-1} after dilution), more intense colors were observed for BC anthocyanins (Fig. S1(C)), which is probably related to the greater color strength of these anthocyanins (37–43 CU/kg) and their greater TAC.

The UV–Vis spectra of GP anthocyanins (Fig. S1(A)) showed maximum absorbance peaks shifting from 520 nm (pH 2 and 3) to about 600 nm (up to pH 9), which is associated with a color change from intense pink to light pink and gray. From pH 10 onwards, a light blue coloration appeared and changed to a more greenish color and, finally, to a yellowish color, which corresponds to pH 12 and 13. According to Nogueira et al. (2024) [9], the color response observed for solutions based on grape pomace extracts is related to the combination of anthocyanins glycosides, like malvidin, delphinidin, and cyanidin; these compounds are flavylium cations, which are red-colored at acidic pH and transform into colorless forms of carbinol pseudo bases at neutral pH. As the pH increases to alkaline values, they transform into blue quinoid bases (pH 8–10), which finally degrade and form yellow chalcones at pH ≥ 12.

Fig. S1(B) shows the color change and the UV–Vis spectra of SP anthocyanins. Their lower TAC and color strength yield less intense colors observed in the image. Despite that, the color change with increasing pH values is noticeable, with the anthocyanins going from light pink at more acidic pH values to purple at more alkaline pH and, finally, to yellow at higher pH (12 and 13). Such variation in color corresponds to the differences observed in the UV–Vis absorption spectra, especially related to the shift to higher wavelengths of maximum absorbance at higher pH values (from 500 to 580 nm). The color variation of SP anthocyanins can also be explained by the mechanism previously elucidated for GP anthocyanins, i.e., the reversible structural transformations in the molecules (mainly cyanidin and peonidin forms) due to changes in pH. According to Sohany et al. (2021) [28], the transformations of sweet potato anthocyanins involve, in a first step, the change of flavylium cations (red) to quinoidal anhydrases (purple); in an alkaline medium, the anhydrases change to quinoid bases (blueish) and, finally, to chalcones (yellow).

Finally, Fig. S1(C) shows the UV–Vis spectra and the color variation of BC anthocyanins, the ones with greater TAC and color strength. Again, the shift from 520 to 600 nm observed in the wavelengths of maximum absorbance is related to the change from an intense red color (at acidic pH) to purple, blue, green, and finally, yellowish colorations. The same tendency of color change was reported by Yilmaz & Türker (2024) [30], who investigated the stability of anthocyanins from black carrot extracts when exposed to different pH values and to high temperatures. The results of color variation at different pH show that all anthocyanin solutions in CC-GLY prepared in this study can be used in food deterioration indicator media, especially when under alkaline conditions.

3.2. Nanofibers production and optimization by solution blow spinning

The solution properties are the most critical parameter in nanofiber production techniques such as electrospinning, solution blow spinning, and centrifugal spinning [34]. The electrospinning of cellulose acetate (CA) nanofibers is well-established and typically involves solvent mixtures such as acetone, *N*,*N*-dimethylformamide (DMF), dichloromethane (DCM), methanol (MeOH), *N*,*N*-dimethylacetamide (DMAc), acetic acid, and formic acid [35–38]. These solvent systems are suitable for CA nanofiber production due to their ability to modulate solution parameters, including viscosity, surface tension, and conductivity [39–41]. In addition, the acetate groups in CA exhibit favorable interactions with solvents such as chloroform, methyl chloride, and dioxygen, whereas the hydroxyl groups interact more strongly with DMF, acetone, methanol, and acetic acid [41].

Nevertheless, identifying suitable solutions for CA nanofiber production via SBS has proven to be more challenging. For instance, CA solutions containing acetone/DMF or acetone/acetic acid tend to form films rather than fibers, resulting in limited fiber formation [42]. In our experiments, when CA solutions containing chloroform, methanol, DCM, and acetone were processed via SBS, tubular structures (~1–2 mm wide) grew at the needle tip until it collapsed due to wind turbulence, failing to form the desired stretched fibers. This tube consisted of a dry outer layer but retained a high solvent concentration internally, suggesting that the air dragging force was insufficient to stretch the solution, leading to solvent evaporation primarily at the tube surface. This phenomenon was attributed to the high surface tension caused by strong intermolecular interactions, despite the solution moderate viscosity

[41,43,44]. Thus, given the nature of the SBS technique of coaxial air entrainment to stretch the fiber solution and form the fibers, further weakening of the intermolecular bonds of the CA was necessary.

To address this, nanofibers were produced via SBS using CA/polyethylene oxide (PEO) co-solutions, followed by PEO removal in deionized water [45,46]. The 1:1 CA/PEO solution ratio was empirically selected as the minimum proportion required to ensure jet stability and continuous fiber formation by the SBS technique. Lower PEO contents led to unstable jets and incomplete fiber formation. PEO acted solely as a temporary spinning aid, as its flexible chains facilitated the stretching of the CA/PEO solution by reducing the effective intermolecular interactions and elastic resistance of the CA-rich system, and was subsequently removed by water washing, not being intended as a component of the final material [45].

In addition to solution composition, air pressure is a critical parameter governing jet stability and fiber formation in SBS procedures [14]. An air pressure of 2 bar was selected to provide sufficient aerodynamic force to overcome the strong intermolecular interactions and

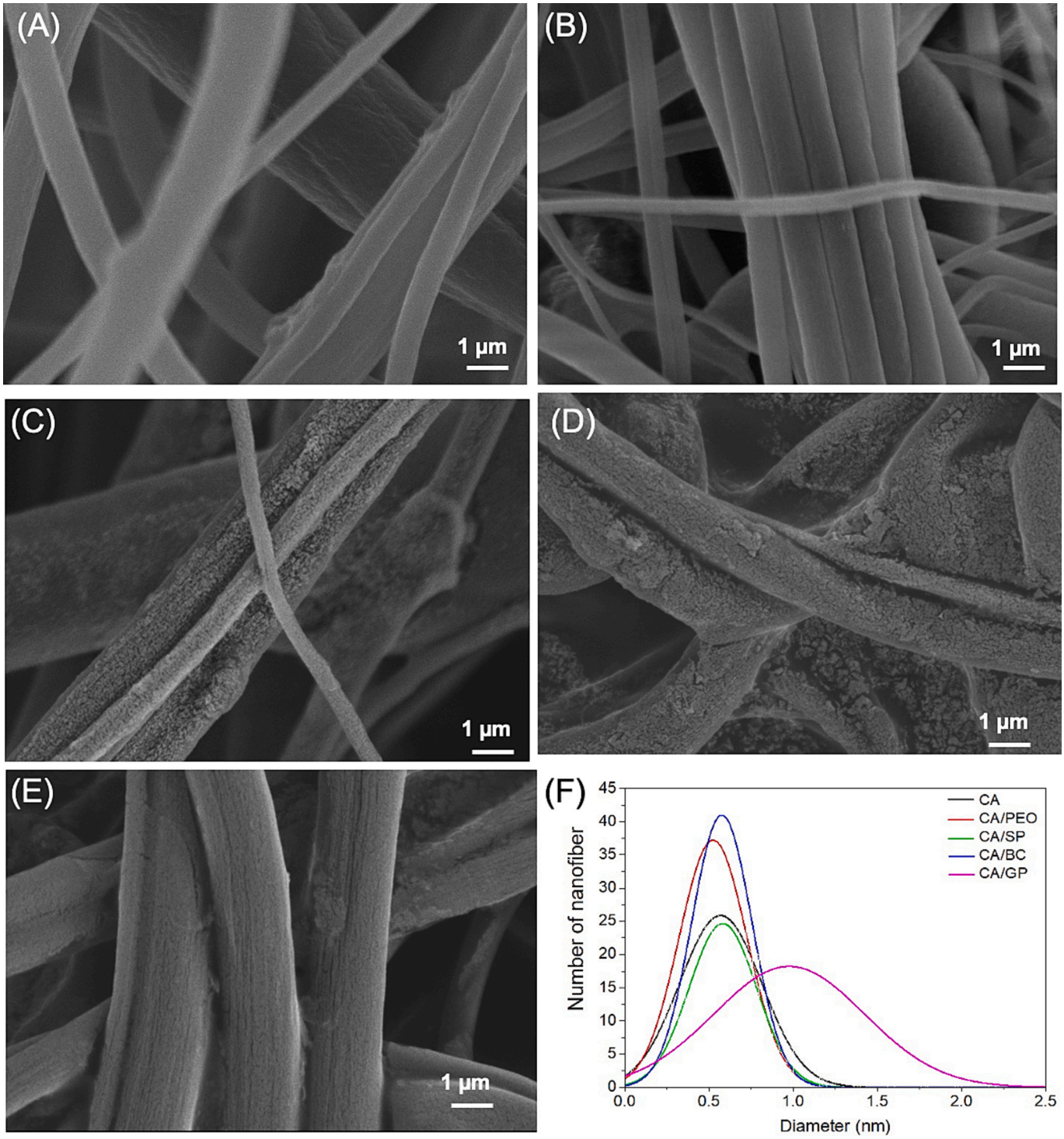

Fig. 2. SEM images of the CA-PEO nanofibers (A) and CA fibers (B) after PEO removal. In (C), (D), and (E), CA nanofibers after incorporation of SP, BC, and GP anthocyanins, respectively. Magnifications of 10,000×. (F) Normal curve of histograms with size distribution of nanofibers' diameters.

surface tension of cellulose acetate-rich solutions, which are known to hinder CA fiber formation by SBS and promote the formation of tubular or film-like structures at the nozzle [42,44]. Although the incorporation of PEO facilitated jet elongation by weakening these interactions, pressures below 2 bar were insufficient to ensure continuous fiber formation, while higher pressures increased jet instability and led to a deposition not uniform. Therefore, 2 bar represents a balanced condition that enables stable stretching of CA/PEO solutions and reproducible formation of homogeneous nanofibrous mats, which agrees with previous SBS studies on CA-based systems [46].

After optimization of the composition, the CA nanofibrous mats were immersed into pectin-based solutions containing the GP, SP, and BC anthocyanins and CC-GLY, according to the procedure described in section 2.4. The method of anthocyanins incorporation into the mats was optimized by previous assays, such as immersing the nanofibrous mats directly into the CC-GLY solutions, without pectin. Fig. S2 shows the appearance of the CA nanofibers specimens after immersion in a CC-GLY solution with 50 mg mL^{-1} of BC. The incorporation was not uniform throughout the nanofiber specimens as it is corroborated by the presence of discolored regions in almost all of them. This result can be justified by the low affinity of CA for CC-GLY, due to the more hydrophobic nature of the polymer when compared to the great hydrophilic character of the NADES [47]. Thus, the presence of pectin as a carrier medium to increase the affinity of CA by the anthocyanins solubilized in CC-GLY is justified.

Pectin was incorporated into the anthocyanin-NADES system as a functional carrier to enhance pigment retention on the cellulose acetate nanofibers during the post-spinning immersion step. Due to its high density of hydroxyl and carboxyl groups, pectin can establish multiple hydrogen-bonding interactions with anthocyanins, contributing to the formation of a cohesive and hydrophilic coating layer, as commonly reported for polysaccharide-anthocyanin systems [25]. In addition, non-covalent interactions and physical adsorption between pectin and the CA surface are expected to promote adhesion of the pigment-containing layer onto the nanofibers.

Overall, a two-step strategy was adopted for CA-based nanofibers formation, as direct spinning of CA with anthocyanins was hindered by solvent incompatibility and jet instability, while incorporating the pigments prior to PEO removal would likely result in their loss during the aqueous washing step. Therefore, stable CA nanofibers were first obtained by an optimized SBS methodology, followed by anthocyanin incorporation using a pectin-based system containing NADES, which ensured homogeneous coloration and preserved pigment retention.

3.3. Nanofibers characterization

3.3.1. SEM

Fig. 2 (A-F) presents SEM images of CA-PEO, pure CA, and CA-anthocyanins nanofibers and the distribution of nanofibers' diameters can be verified in Fig. 2(F). As shown in Fig. 2(A) and (B), the CA-PEO fibers exhibited an irregular morphology due to PEO incorporation, as expected [46], and the average diameter for CA/PEO nanofibers was 575 ± 244 nm. The morphological investigation revealed that the nanofibers tend to pack in bundles, and the presence of residual solvent can cause the formation of nanofibers' clusters greater than 1 μm. These clusters were not counted in the diameter measurements. The nanofibers' aspect changed after the washing procedure for PEO removal (sample CA, Fig. 2(B)), in such a way the surface appears smoother and less irregular, while no significant changes have been verified in nanofibers' diameters, which were around 580 nm.

The modification with anthocyanins impacted the CA nanofibers' surface morphology. As shown in Figs. 2(C), (D), and (E), after immersing the fibers in the pectin solutions containing SP, BC, and GP anthocyanins, respectively, organic material was adhered onto the fiber surfaces, resulting in increased roughness. The diameter distribution of the samples CA/SP and CA/BC were not significantly impacted by the surface modification procedure, in contrast with the CA/GP sample. It is worth mentioning that the CA/GP nanofiber presented a more uniform and refined appearance, but a wider size distribution than the others (Fig. 2(F)), with larger diameter average, suggesting that the differences in the anthocyanins physical chemistry (as it was confirmed in the previous characterizations of these pigments) influenced the final morphology of the mats. The morphological investigation of CA/GP suggests that the GP anthocyanin is distributed along the nanofibers like a veil, leading to the approximation of the nanofibrous elements, resulting in the formation of larger clusters, reaching diameters as big as 2.5 μm.

3.3.2. FTIR-ATR

The composition of commercial CA, pure and modified CA nanofibers, as well as the interactions between their components, were investigated by FTIR-ATR. Fig. 3(A) shows the FTIR spectra of the materials, which confirmed the presence of the main functional groups of CA and indicated changes due to the incorporation of anthocyanins.

The FTIR spectra of all samples are mainly characterized by the typical absorption bands of cellulose acetate (CA), including the broad O—H stretching band around 335 cm^{-1}, associated with hydroxyl groups present in CA, pectin, and anthocyanin structures; the C—H stretching vibrations in the 2800–3000 cm^{-1} region; and the C═O stretching band at approximately 1735 cm^{-1}, corresponding to carbonyl groups from acetate moieties. The band around 930 cm^{-1} is attributed to C—O and C–O–C skeletal vibrations associated with the polysaccharide backbone of CA and pectin. Finally, the bands observed at 1235–1240 cm^{-1} and around 1030 cm^{-1} are attributed to C–O–C asymmetric stretching and C—O stretching vibrations associated with polysaccharide-related structures, respectively [48–50]. These assignments are consistent with previous reports on cellulose acetate films and nanofibrous materials [51–54]. The main differences observed between commercial CA and CA nanofibers arise from the presence of residual polyethylene oxide (PEO) used as an auxiliar for CA spinning. The arisen of doublet peaks in the region of 1035–1109 cm^{-1} is resultant of the combination PEO and CA signals [55,56]. Bands appearing in the 1340 cm^{-1} can be related to O—H bending and 2874 cm^{-1} correspond to symmetric and asymmetric stretching modes of CH_2 groups [57,58].

Differences among CA nanofibers and CA modified with anthocyanins are subtle, which is expected due to the low pigment content and surface-localized functionalization. The main spectral indications of anthocyanin presence are: (i) the band near 1600 cm^{-1}, related to C═C stretching vibrations of aromatic rings, indicative of phenolic compounds; and (ii) slight changes in the O—H stretching region around 3395 cm^{-1} [49,51–54,59]. The broadening and minor shifts observed in the O—H stretching region and in carbonyl-related bands after functionalization are consistent with the introduction of additional hydrogen-bonding interactions associated with pectin and anthocyanins. These spectral features, together with the surface coverage observed in SEM images, suggest that anthocyanin incorporation occurred predominantly through physical interactions, mainly hydrogen bonding, rather than through covalent bonding [49].

3.3.3. Thermal properties

TGA analysis of commercial CA and CA nanofibrous mats with and without anthocyanins resulted in the thermograms displayed in Figs. 3 (B) and (C). The information regarding T_{onset} and residual matter are described in Table 1. A simpler degradation profile is verified for commercial CA, in comparison with CA nanofibers and nanofibrous mats containing anthocyanins. Commercial CA profile is characterized by fewer thermal decomposition events and a lower residual mass at 600 °C. This behavior is attributed to its higher chemical homogeneity and absence of polyethylene oxide (PEO). In this direction, commercial CA thermal degradation profile is marked by two main events of weight loss, the first one at 298 °C, related to the main degradation of the CA backbone, followed by deacetylation, while the second event, between

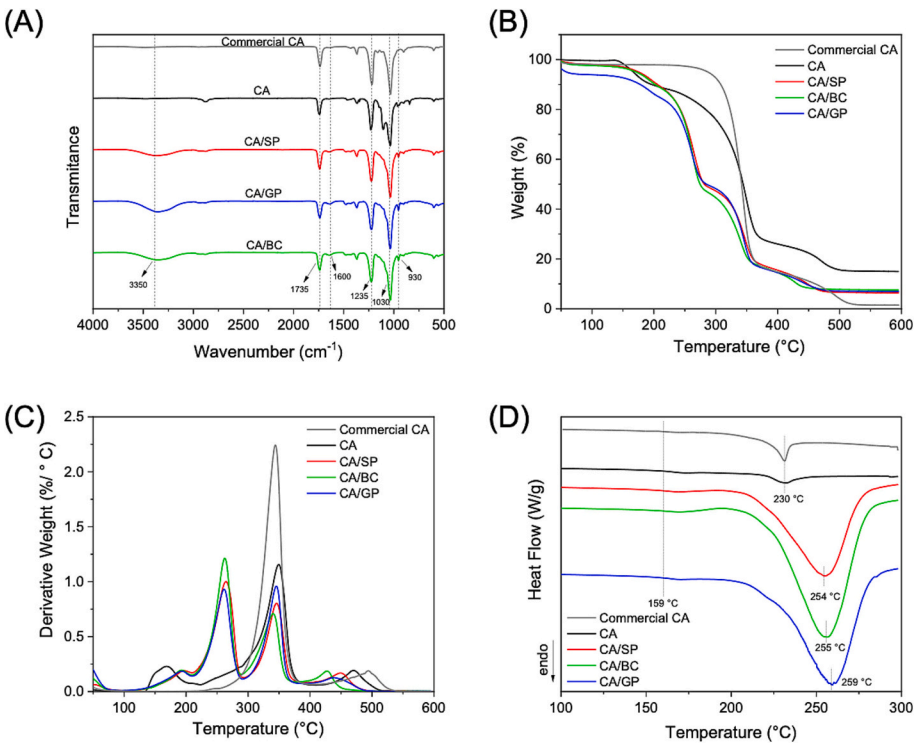

Fig. 3. Characterization of chemical composition of commercial CA, pure and modified CA nanofibers, as well as the interactions between their components: (A) FTIR spectra, (B) TGA thermograms and (C) their corresponding DTG curves, and (D) DSC second heating curves.

Table 1
Thermal properties of commercial CA and CA-based nanofibrous mats, including onset degradation temperatures (T_{onset}), residual matter percentages, glass transition temperatures (T_g), melting temperatures (T_m), and melting enthalpy (ΔH_m). Water-related properties of the CA-based nanofibrous mats: WCA (°) and water-induced mass loss (%).

Sample	Average diameter (nm)	T_{onset1} (°C)	T_{onset2} (°C)	T_{onset3} (°C)	T_{onset4} (°C)	Residual matter (%)	T_g (°C)	T_m (°C)	AH_m (J g^{-1})
Commercial CA	–	–	–	298	477	1.5	162	232	10.9
Nanofibrous mats									
CA	528 ± 200	147	–	287	443	14.9	159	230	5.87
CA/GP	589 ± 198	153	230	317	426	6.9	154	259	210.8
CA/SP	582 ± 176	162	233	317	432	6.38	159	254	178.0
CA/BC	981 ± 449	160	235	315	410	7.5	157	255	265.2
Sample		**WCA (°)**				**Water-induced mass loss (%)**			
CA		60.93 ± 3.89[b]				10.26 ± 2.66[c]			
CA/GP		 70.34 ± 5.01[a]				48.79 ± 2.00[b]			
CA/SP		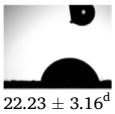 22.23 ± 3.16[d]				50.29 ± 3.92[b]			
CA/BC		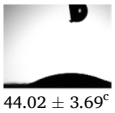 44.02 ± 3.69[c]				62.08 ± 0.74[a]			

Values in the same row with different superscript letters indicate statistically different samples by ANOVA and Tukey ($p \leq 0.05$). Samples: CA – cellulose acetate, CA/GP: cellulose acetate with grape pomace anthocyanins, CA/SP: cellulose acetate with sweet potatoes anthocyanins, and CA/BC: cellulose acetate with black carrots anthocyanins.

400 and 500 °C, describes the carbonization of residual matter [49,51–54]. In contrast, CA nanofibers exhibit other mass-loss steps, which are associated with the presence of residual solvents, residual PEO and with the heterogeneous nanofibrous morphology. The first additional weight loss event, in comparison with commercial CA, occurs in the region between 100 and 200 °C and is associated with water evaporation and decomposition of volatile organic compounds. Literature describes that pure PEO decomposes at 350–400 °C, while no event has been verified specifically at this point, the presence of residual PEO can be reflected in the different profile of the main event of CA degradation, in the case of CA nanofibers [60].

The thermograms of the anthocyanin-containing samples showed some differences compared to the neat CA. In the first step, corresponding to the T_{onset1} of neat CA, a less pronounced weight loss was observed, suggesting that the incorporation of anthocyanins on the outer surface of the nanofibers (as confirmed by SEM analysis) may have provided a certain degree of protection to the pure CA. The thermal degradation of anthocyanins occurs around 60 °C, in an event associated with their less heat-resistant nature [61,62]. The degradation process involves their conversion into chalcone structures, followed by fragmentation into volatile phenolic compounds and carbon dioxide, thus contributing to a lower final weight residue after the carbonization steps [63]. Moreover, weight losses at 25–140, 140–290, and 290–700 °C corroborate with the thermal degradation profile of pectin, a biopolymer present in the anthocyanin extract used in our study [64]. The main difference between TG/dTG profiles regards the region of 200–400 °C. In this temperature range, where only one event was observed for neat CA, two distinct events were detected for the CA/anthocyanin samples. These are more clearly visible in the dTG curves shown in Fig. 3(C) and in the corresponding T_{onset2} and T_{onset3} values presented in Table 1. The weight loss associated with T_{onset2} can therefore be attributed to the degradation of pectin and anthocyanin compounds.

The event corresponding to the main degradation of CA, described in Table 1 as T_{onset3}, was slightly postponed, which can be related to the presence of anthocyanins and their carbonaceous residues. Finally, the last event, in the range of 400–500 °C, corresponding to the pyrolytic decomposition and volatilization of compounds, was anticipated for the samples containing anthocyanins and pectin, which must be related to their lower thermal stability.

DSC analysis was performed to monitor potential interactions between the CA polymeric matrix and the incorporated anthocyanins extracts. Second heating curves are presented in Fig. 3(D) and the values of glass transition temperature (T_g), melting temperature (T_m), and melting enthalpy (ΔH_m) are described in Table 1. The incorporation of anthocyanins did not affect the CA T_g, but led to relevant increases in T_m values, suggesting interactions between the CA matrix and the different anthocyanins extracts [49].

Initially, comparing the profiles of commercial CA and pure CA nanofibrous mats, it is observable that they are similar and can be described by a high T_g (~ 160 °C), a T_m of 230 °C [65,66], and a shallow melting valley, reflecting the low melting enthalpy known for cellulose esters [67]. The main difference between commercial cellulose acetate and CA nanofibers lies in the melting enthalpy (ΔH_m). No distinct melting peak associated with polyethylene oxide (PEO) is detected, indicating that the residual PEO is present in low content and in a highly dispersed or amorphous state, likely due to strong intermolecular interactions with CA that hinder its crystallization. The superior value of ΔH_m observed for commercial CA reflects a higher degree of crystalline order and more stable crystalline domains. In contrast, CA nanofibers exhibit a reduced melting enthalpy, which is attributed to the disruption of crystalline packing caused by the solubilization and the fast solvent evaporation, chain stretching during spinning, and the presence of residual PEO [68].

Distinct changes in the thermal profile of CA nanofibrous mats were observed after incorporation of anthocyanins, followed by differences in the shape of the melting signal and, most notably, in the ΔH_m values for anthocyanin-loaded samples, in contrast to pure CA. This increase in enthalpy reflects interactions between CA and anthocyanins, which may have enhanced the CA chain packing by hydrogen bonds, indicating a substantial increase in the ordered phase or crystallinity, as supported by FTIR data. These results indicate the occurrence of strong interactions between anthocyanins and CA chemical groups, such as hydrogen bonding and π–π stacking [49]. This behavior may be attributed to the nucleating effect of anthocyanins, which possibly promoted local rearrangement of CA chains, favoring the formation of more stable crystalline domains, which demanded more energy to melt [59].

3.3.4. Water-related properties

The study of water-related properties of CA-based nanofibrous mats, with and without anthocyanins, began with the measurement of their hydrophilicity, based on the determination of the contact angle between water droplets and the surface of the fibers. Table 1 shows the WCA values found for each nanofibrous mat, measured in the second frame after the water droplet contacted the fiber surface (i.e., approximately 0.5 s after the contact). Even though the WCA was recorded at the beginning of the contact, this time interval was chosen and standardized for all fibers due to the rapid water droplets absorption by the CA fibers, especially for the more hydrophilic ones, which prevented accurate measurements at longer time intervals.

All the samples showed WCA values lower than 90°, which reflects the hydrophilic character typical of CA. According to the literature, CA-based materials usually present WCA values between 60 and 70° [69], which is consistent with the value found in this study for the sample without anthocyanins. The addition of anthocyanins extracts led to different effects, according to the anthocyanin nature: GP extract addition increased the WCA of CA nanofibrous mats to 70.34 ± 5.01°, decreasing its hydrophilic character. For the other two anthocyanins, on the other hand, WCA values decreased substantially, which indicates that they have increased the wettability and the hydrophilicity of CA mats.

Several effects can play a role in the wettability of polymer-based fibers: the addition of molecules with functional groups capable of interacting with water, as is the case of anthocyanins, usually tend to increase wettability and, consequently, decrease WCA values [2]. Nevertheless, the added compounds can also interact with CA, decreasing the interactions between the polymer chains with water, and, consequently, decreasing wettability. These compounds can also increase the roughness of the fibers surface, leading to more pores and voids with air incorporated, which may also increase hydrophobicity [1]. Furthermore, the presence of pectin and CC-GLY in the nanofibrous mats coated with anthocyanins can also affect the material's wettability. Pectin interacts with cellulose acetate through hydrogen bonding and electrostatic interactions, especially at their surface levels. As explained in section 2.2, this was one of the reasons for selecting this polymer to increase the affinity between CC-GLY-based anthocyanin solutions and cellulose acetate [70]. CC-GLY-based NADES, in turn, can also interact with cellulose chains through hydrogen bonds [47], if there are still available sites for binding.

Therefore, this variety of factors explains the distinct effects brought about by the incorporation of anthocyanins into CA fibers. In particular, the contrasting WCA trends can be attributed to the combined influence of anthocyanin chemical characteristics (polarity and molecular organization), pectin adsorption efficiency, and fiber surface morphology. GP anthocyanins may have interacted more with CA, leading to smoother fibers (as observed in the SEM images) and decreasing the availability of hydrophilic sites at the surface, which resulted in higher WCA values. The other anthocyanins, in turn, may have promoted a more effective surface coverage by the pectin-NADES system, increasing surface roughness and the exposure of hydrophilic functional groups, thereby enhancing water affinity. This interpretation is consistent with the greater decrease in WCA observed for CA/SP and CA/BC samples, particularly for SP anthocyanins, despite their lower TAC.

To quantitatively assess the incorporation of the pectin-NADES-anthocyanin system onto the nanofibrous mats, the mass per unit area was determined gravimetrically. Neat CA nanofibers presented an average mass of 4.37 ± 0.92^{c} mg cm^{-2}, while functionalized samples showed higher values depending on the anthocyanin source, namely 7.07 ± 0.77^{b} mg cm^{-2} for CA/GP, 9.95 ± 0.25^{a} mg cm^{-2} for CA/BC, and 12.8 ± 0.30^{a} mg cm^{-2} for CA/SP (different letters indicate statistically significant differences, $p \leq 0.05$).

The different mass per unit area values indicate that the incorporation efficiency of the functional system strongly depends on the anthocyanin source. The higher mass gain observed for CA/SP is consistent with its pronounced effect on surface wettability and water sensitivity, suggesting a more extensive surface coverage by the pectin-NADES system. In contrast, the lower mass gain of CA/GP agrees with its smoother morphology and higher WCA values.

Table 1 shows the water-induced mass loss of the CA-based nanofibrous mats, with and without anthocyanins. Although cellulose acetate is not chemically soluble in water, this assay was applied to evaluate the structural integrity and water sensitivity of the fibrous mats upon aqueous exposure [71]. Neat CA samples exhibited a relatively low mass loss ($10.26 \pm 2.66\%$), confirming the intrinsic water resistance of the cellulose acetate matrix. In contrast, anthocyanin-containing samples showed significantly higher mass loss values, reaching $62.08 \pm 0.74\%$ for CA/BC. This increase is attributed to the incorporation of hydrophilic components at or near the fiber surface, including anthocyanins, pectin, and NADES constituents, which increased the availability of functional groups capable of interacting with water, as supported by the weight gain results [72].

Moreover, as supported by the WCA results, the presence of NADES as a carrier medium for anthocyanins in the pectin-based system further enhances water sensitivity by promoting water penetration into the fiber network. Similar behavior has been reported by Thakur et al. (2022) [18], who observed increased mass loss in polyvinyl alcohol films containing anthocyanins solubilized in natural deep eutectic solvents.

Importantly, the observed mass loss does not indicate dissolution of the cellulose acetate backbone, but rather reflects the presence and release of hydrophilic, surface-associated components and the increased water sensitivity induced by functionalization. Strategies such as post-spinning cross-linking, surface coating, or incorporation of hydrophobic barrier layers could be explored to reduce water sensitivity while preserving the colorimetric response. From an application perspective, the increased mass loss in water observed for the materials developed in this study does not represent a drawback, since the colorimetric sensor operates through exposure to volatile compounds in the package headspace and does not require direct contact with aqueous food matrices, as demonstrated in the following section.

3.4. pH sensitivity

3.4.1. pH responsiveness

Fig. 4(A) shows the procedure of (i) immersion of the CA nanofibrous mats into pectin-based anthocyanins solutions containing CC-GLY, and (ii) the final aspect of the mats after dried. All samples showed homogeneous coloration, with no visible regions in which anthocyanin solutions were not incorporated, confirming the successful use of CC-GLY and pectin for the pigments incorporation. The nanofibrous mats were then immersed in solutions with different pH for 30 s each, and Fig. 4(B), (C), and (D) shows the aspect of the materials after removal from the solutions. The three samples showed visible color variations from the acidic to the basic medium, with changes from pink to greenish/bluish. These results confirm that the color variation observed for the anthocyanins, as shown in section 3.1, is maintained when they are incorporated into CA-based materials.

CA/BC fibers presented a more visible color variation at lower pH values, becoming greenish at pH 6, while the others effectively changed color only at pH > 10. Table 2 shows the L*, a*, b*, and ΔE parameters for each sample at each pH value analyzed, as well as before being immersed in the solutions (control). In general, the fiber with the lowest ΔE at higher pH values was CA/SP (from 7.65 ± 0.24 at pH 6 to 14.99 ± 0.08 at pH 12). Although they are the lowest, these ΔE values are greater than 5 and ensure that the color variation for this fiber to be visible to the naked eye [5]. CA/BC was the sample with the highest ΔE at higher pH values (from 18.08 ± 0.42 at pH 6 to 24.60 ± 0.50 at pH 12), which agrees with its lowest b* values (blue-yellow component of the color), which, when negative, relate to a stronger blue chromaticity.

The differences in pH responsiveness observed among the CA-based nanofibrous sensors can be interpreted in light of the structural characteristics of the anthocyanins discussed in section 3.1. In particular, the more pronounced and earlier color changes observed for the CA/BC sensor are consistent with the higher degree of acylation and structural complexity typically reported for black carrot anthocyanins, which favor intramolecular copigmentation and contribute to improved color persistence under alkaline conditions [26,27]. In contrast, the comparatively lower ΔE values observed for CA/GP and CA/SP sensors may be associated with differences in pigment substitution patterns and color strength, which can limit the intensity and stability of chromatic transitions at higher pH values [12,25]. These structure-function relationships help rationalize the different pH sensitivities observed among the sensors and reinforce the relevance of anthocyanin source selection for optimizing colorimetric performance.

3.4.2. Colorimetric responses to volatile ammonia

Protein-rich foods (like chicken, salmon, meat, eggs, among others) degrade by producing volatile nitrogen compounds such as ammonia and biogenic amines [7]. Therefore, the pH of spoiled foods generally increases, which makes anthocyanins potential indicators of their spoilage [73]. As shown in section 3.4.1, all anthocyanins in this study showed more pronounced color changes at higher pH values, which encouraged the study of their response when exposed to environments where volatile ammonia is present. As previously stated, the sensors do not necessarily need to be in contact with the food to indicate spoilage, and their exposure to the headspace of the spoiled food should be enough to promote the color change and indicate to the consumer, in a safe manner, that the food is no longer suitable for consumption [74].

Fig. 4(E) shows the difference in coloration observed for the CA-based nanofibrous mats containing anthocyanins after exposure to the headspace of distilled water (control) and a basic (ammonia vapor) medium. All fibers changed color in less than 1 min of exposure to ammonia vapor, which is desirable for a colorimetric sensor. CA/GP and CA/BC fibers changed from pink (control) to greenish/bluish tones, while the change observed for the CA/SP fiber was to a more grayish tone.

The values of L*, a*, and b* for each fiber in each of the media are found in Table 2. From these parameters, the total color difference between the samples in the control and in the alkaline medium was calculated; all ΔE values were greater than 5, which implies that all three samples led to color changes that can be clearly distinguished by naked eye [5,74]. CA/BC was the sample with the greatest ΔE (37.78 ± 2.19) and, therefore, the most sensitive to the exposure to alkaline environments. This result is in line with the previous results of color change for BC anthocyanin and for the CA/BC sample immersion in different pH solutions, which are all probably related to the greater TAC and color strength of BC, when compared to the other anthocyanins.

The ΔE values found in this study are similar or even higher than others reported in the literature that used CA-based materials for intelligent packaging. Freitas et al. (2020) [2], for instance, prepared CA films containing red cabbage extract, and observed that the total color variation of the films under exposure to volatile ammonia was directly related to the extract concentration. The film with the highest concentration of extract led to a ΔE value of ~11, after 25 min of exposure. Zhang et al. (2022) [5], in turn, developed cellulose acetate membranes with *Perilla frutescens* (L.) Britt. anthocyanins and chamomile essential

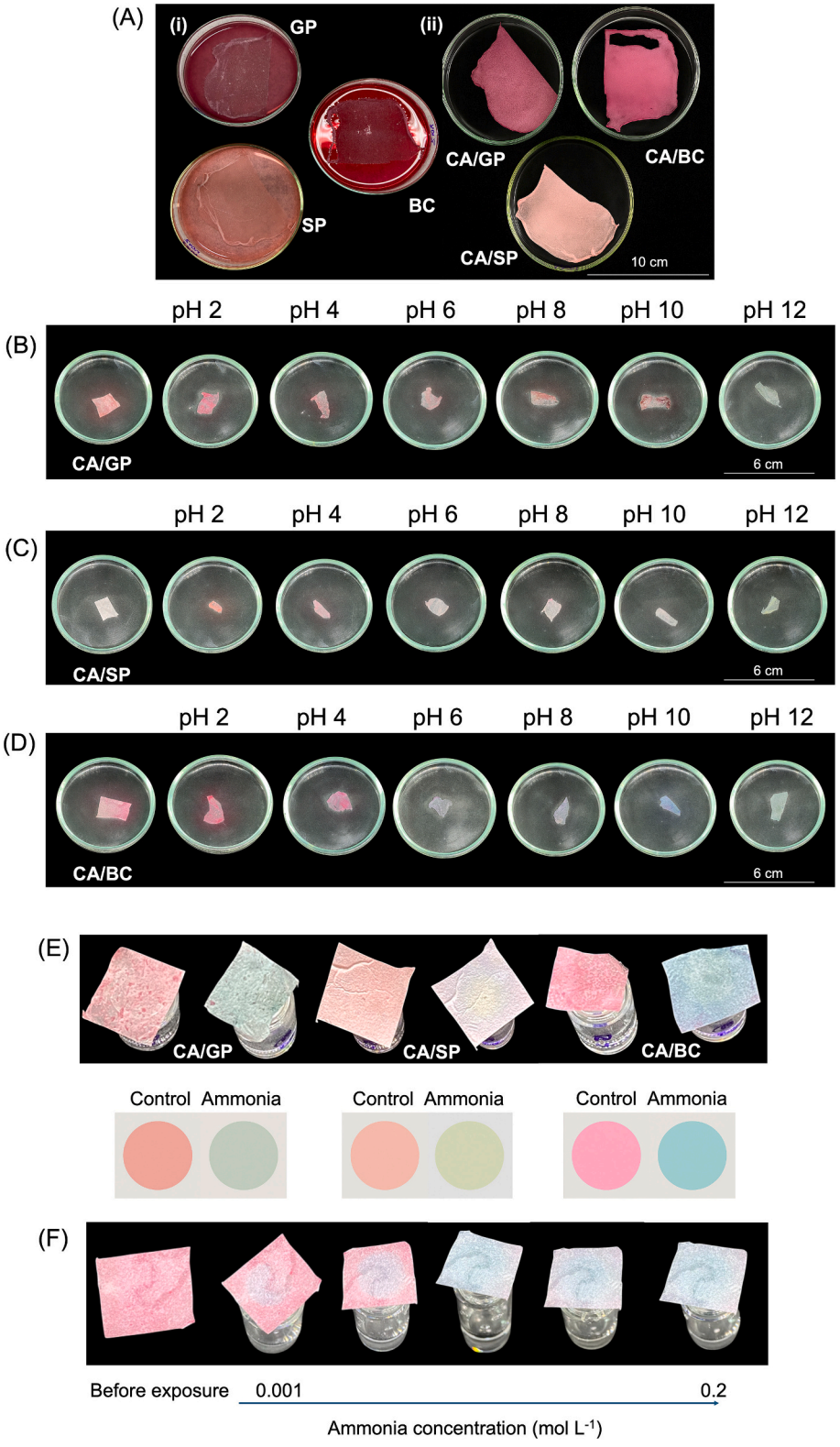

Fig. 4. (A) Immersion of the CA nanofibrous mats into pectin-based anthocyanins solutions containing CC-GLY (i), and the final aspect of the nanofibrous mats after dried (ii). Color change after immersion in pH 2–12 solutions for: (B) CA/GP, (C) CA/SP, and (D) CA/BC samples. (E) Color change of the samples after exposure to the headspace of distilled water (control) and concentrated ammonium hydroxide environments for 1 min. (F) Color change of CA/BC after exposure to the headspace of different ammonium hydroxide concentrations for 5 min.

Table 2
Color parameters (L*, a* and b*) and total color variation (ΔE) of the CA-based nanofibrous mats with anthocyanins before and after immersion in pH 2–12 solutions; color parameters (L*, a* and b*) and ΔE of the CA-based nanofibrous mats with anthocyanins after exposure to the headspace of distilled water (control) and volatile ammonia.

CA/GP	Control	pH 2	pH 4	pH 6	pH 8	pH 10	pH 12
L*	74.88 ± 0.06^{a}	68.22 ± 0.07^{c}	68.86 ± 0.27^{c}	72.44 ± 0.22^{b}	69.40 ± 0.40^{c}	65.30 ± 1.10^{d}	73.21 ± 0.37^{b}
a*	16.12 ± 0.09^{b}	21.21 ± 0.26^{a}	8.84 ± 0.54^{c}	6.81 ± 0.43^{d}	8.82 ± 0.38^{c}	9.28 ± 0.71^{c}	−5.47 ± 0.02^{e}
b*	8.35 ± 0.26^{a}	2.45 ± 0.09^{f}	3.86 ± 0.11^{e}	3.78 ± 0.13^{e}	7.60 ± 0.10^{b}	6.09 ± 0.32^{c}	5.35 ± 0.06^{d}
ΔE	–	10.11 ± 0.12^{c,d}	10.44 ± 0.39^{c}	10.63 ± 0.48^{c}	9.21 ± 0.13^{d}	12.06 ± 0.45^{b}	21.89 ± 0.05^{a}

CA/SP	Control	pH 2	pH 4	pH 6	pH 8	pH 10	pH 12
L*	87.57 ± 0.19^{a}	74.83 ± 0.07^{f}	77.93 ± 0.02^{d}	80.04 ± 0.03^{c}	80.94 ± 0.05^{b}	80.47 ± 0.05^{b,c}	75.92 ± 0.34^{e}
a*	0.74 ± 0.03^{d}	16.94 ± 0.16^{a}	9.99 ± 0.10^{b}	1.21 ± 0.05^{c}	1.33 ± 0.01^{c}	−0.02 ± 0.03^{e}	−7.07 ± 0.10^{f}
b*	3.43 ± 0.02^{c}	12.89 ± 0.18^{a}	2.04 ± 0.04^{f}	2.38 ± 0.04^{e}	2.86 ± 0.03^{d}	2.83 ± 0.07^{d}	8.96 ± 0.16^{b}
ΔE	–	22.68 ± 0.09^{a}	13.44 ± 0.15^{c}	7.65 ± 0.24^{d}	6.68 ± 0.15^{e}	7.17 ± 0.20^{d,e}	14.99 ± 0.08^{b}

CA/BC	Control	pH 2	pH 4	pH 6	pH 8	pH 10	pH 12
L*	74.77 ± 0.18^{b}	66.98 ± 0.11^{f}	66.54 ± 0.18^{f}	71.49 ± 0.16^{d}	72.22 ± 0.09^{c}	70.78 ± 0.31^{e}	76.86 ± 0.08^{a}
a*	17.74 ± 0.44^{b}	21.74 ± 0.32^{a}	20.51 ± 1.55^{a}	0.30 ± 0.06^{c}	1.00 ± 0.11^{c}	−0.87 ± 0.37^{c}	−6.68 ± 0.04^{d}
b*	1.89 ± 0.10^{a,b}	1.64 ± 0.13^{b}	−3.53 ± 0.08^{c}	−1.57 ± 0.09^{b,c}	−3.48 ± 0.14^{c}	−13.18 ± 0.10^{d}	4.02 ± 0.10^{a}
ΔE	–	8.77 ± 0.28^{d}	10.29 ± 0.27^{c}	18.08 ± 0.42^{b}	17.77 ± 0.23^{b}	24.28 ± 0.07^{a}	24.60 ± 0.50^{a}

Sample	CA/GP		CA/SP		CA/BC	
	Control	Volatile ammonia	Control	Volatile ammonia	Control	Volatile ammonia
L*	79.25 ± 2.83^{a}	85.11 ± 1.37^{a}	84.45 ± 3.73^{a}	92.68 ± 0.80^{a}	77.21 ± 0.71^{b}	85.35 ± 1.81^{a}
a*	16.89 ± 0.32^{a}	−6.49 ± 0.09^{b}	9.31 ± 3.30^{a}	−2.92 ± 0.28^{b}	28.93 ± 1.30^{a}	−7.36 ± 1.19^{b}
b*	5.91 ± 0.21^{a}	4.30 ± 0.87^{a}	8.40 ± 0.91^{a}	5.16 ± 0.08^{b}	2.42 ± 0.41^{a}	−3.18 ± 2.40^{a}
ΔE	24.21 ± 0.48^{b}		13.98 ± 3.29^{c}		37.78 ± 2.19^{a}	

Values in the same row with different superscript letters indicate statistically different samples by ANOVA and Tukey ($p \leq 0.05$). For the L*, a*, and b* parameters of the materials after exposure to the headspace of distilled water and volatile ammonia, values in the same row for the same sample, with different superscript letters, indicate statistically different samples by ANOVA and Tukey ($p \leq 0.05$); for the ΔE parameter, values in the same row with different superscript letters indicate statistically different samples by ANOVA and Tukey ($p \leq 0.05$). Samples: CA – cellulose acetate, CA/GP: cellulose acetate with grape pomace anthocyanins, CA/SP: cellulose acetate with sweet potatoes anthocyanins, and CA/BC: cellulose acetate with black carrots anthocyanins.

oil via electrospinning, and reported a ΔE value of ~54, after 32 s of exposure of their films to 5% (*v*/v) volatile ammonia. Similarly, Liu et al. (2022) [59] reported electrospun cellulose acetate-anthocyanin nanofibers exhibiting clear and rapid colorimetric responses to pH variations, further confirming ES as the most commonly used technique for producing CA-based halochromic sensors. In this context, the use of SBS represents a relevant methodological advance for the development of CA-based halochromic sensors. Compared to solvent casting and ES, SBS enables the rapid fabrication of highly porous nanofibrous mats without the use of high-voltage electric fields, combining high surface area with improved scalability. These characteristics are particularly advantageous for colorimetric sensing applications, as they favor fast analyte diffusion and prompt visual response [2,14]. To the best of our knowledge, the use of SBS to produce cellulose acetate-anthocyanin nanofibrous sensors for intelligent packaging applications remains scarcely explored, highlighting the novelty of the present approach.

3.4.2.1. Sensor-level response mechanism. At the sensor level, the colorimetric response of the CA-based nanofibrous mats can be explained by the penetration of ammonia vapor into the nanofibrous mat through diffusion within its open and porous structure, reaching anthocyanins located at or near the fiber surface [71]. The nanofibrous morphology produced by SBS provides a large specific surface area and interconnected pores, which reduce diffusion resistance and contribute to the response observed experimentally, as commonly reported for nanofibrous sensing materials [14,71].

In addition, surface roughness and increased hydrophilicity after functionalization, as evidenced by SEM results and by the decrease in WCA values, facilitate the adsorption of ammonia molecules and their interaction with surface-associated anthocyanins, which is consistent with previous reports on halochromic polymer-based sensors [5,47]. These combined structural and surface characteristics explain the visually distinguishable color change upon exposure to alkaline vapors.

Regarding reversibility, Fig. S3 shows the appearance of the nanofibrous mats before being exposed to concentrated ammonia vapor and 10 min after being removed from ammonia exposure, a proof-of-concept about the degree of reversibility of the developed materials. The difference in the color of the fibers is noticeable and shows that they do not return to their original color after being exposed to the alkaline environment, another desirable feature of a food spoilage sensor. The irreversible color change under ambient conditions can be associated with deprotonation of anthocyanins under alkaline conditions and limited reprotonation after removal from the vapor environment, as also observed in CA-based freshness indicators reported in the literature [5,74]. Thus, if the contact between the sensor and the packaging containing the spoiled food is interrupted for some reason, the material will still present a different coloration from the original, indicating that the spoilage has occurred.

3.4.2.2. LOD and LOQ determination. Due to its greater response when in contact with volatile ammonia (ΔE of 37.78 ± 2.19), CA/BC was selected to continue the study of color change as a function of ammonia concentration (Fig. 4(F)), aiming to determine the perceptual limits of quantification and detection (LOQ and LOD) for this phenomenon. LOD was defined as the lowest concentration of ammonia that led to a ΔE of 1 (typically considered the threshold of human perception for color variation), while LOQ was defined as the lowest concentration of ammonia that led to a ΔE of 3 (when the color is visually distinct to the human eye

[74,75].

The equation obtained for the linear region of the ΔE versus ammonium hydroxide concentration curve was $y = 0.2815\times + 3.7438$, with an R^2 of 0.9855. The perceptual LOD and LOQ values calculated from the equation were $(1.73 \pm 0.33) \times 10^{-6}$ and $(8.42 \pm 1.05) \times 10^{-5}$ mol L^{-1}, respectively. Thus, a 5-min exposure of the CA/BC fiber in a solution with a concentration above 1.73 × 10–6 mol L^{-1} of ammonia (about 0.06 ppm) leads to a $\Delta E \geq 1$, the threshold of human perception, while a concentration greater than 8.42 × 10–5 mol L^{-1} (about 3 ppm) leads to a $\Delta E \geq 3$, ensuring that the difference in coloration is clearly perceived by the human eye. Similar values of LOD and LOQ for CA-based freshness indicators have been reported by Lee & Shin (2019) [35]. In a broader context, comparable perceptual detection limits based on visual color change have also been described for polymeric colorimetric indicators targeting volatile basic nitrogen compounds. For example, Wells et al. (2019) [27] developed plastic film indicators for fish spoilage detection and reported clear visual responses at low ammonia concentrations, while Ma et al. (2021) [74] highlighted that perceptual thresholds based on ΔE values are widely adopted to define LOD and LOQ in colorimetric freshness sensors. Together, these studies support the suitability and relevance of the sensitivity achieved by the CA/BC nanofibrous mats developed in the present study.

Considering the intended application of the proposed sensor in food packaging systems, safety and regulatory aspects must also be briefly considered. The proposed colorimetric sensor is designed to operate in the package headspace without direct contact with food. In addition, the materials employed, including cellulose acetate, pectin, and natural anthocyanins, are widely reported in food-related, biodegradable, or packaging applications, while natural deep eutectic solvents (NADES) have been increasingly explored as greener alternatives to conventional organic solvents [14,71]. Nevertheless, before practical implementation, comprehensive toxicological assessment, migration testing under relevant packaging conditions, and compliance with food-contact material regulations would be required.

3.4.3. *Proof-of-concept in real food packaging*

The colorimetric response of the sensors under real food packaging conditions was evaluated using fresh raw salmon samples stored under refrigerated (4 °C) and ambient (25 °C) conditions. Fig. 5 illustrates the visual appearance of the containers, salmon samples, and sensors at representative storage times.

For samples stored at room temperature (25 °C), the CA/BC mats exhibited a pronounced and progressive color change over time. A complete color transition from the initial pink tone to a bluish/grayish coloration was observed after 48 h of storage. This visual change corresponded to a total color difference (ΔE) of 28.49 ± 1.04 relative to the initial time point. At this stage, the salmon samples were visibly deteriorated, confirming the occurrence of spoilage-related processes and the release of volatile basic compounds into the package headspace.

In contrast, the mats exposed to the headspace of salmon samples stored under refrigeration (4 °C) showed significantly slower color evolution. After 48 h, the sensors retained a predominantly pink coloration, with a ΔE value of only 9.46 ± 1.93 relative to time zero, indicating limited accumulation of volatile spoilage compounds. A marked color change to a bluish/grayish tone was only observed after prolonged storage, at 144 h, when the ΔE reached 26.52 ± 0.97. This delayed response is consistent with the reduced rate of spoilage under refrigerated conditions.

These results demonstrate that the developed sensors are capable of discriminating between different storage conditions and spoilage rates based solely on headspace exposure, without direct contact with the food. The clear visual contrast and the significant differences in ΔE

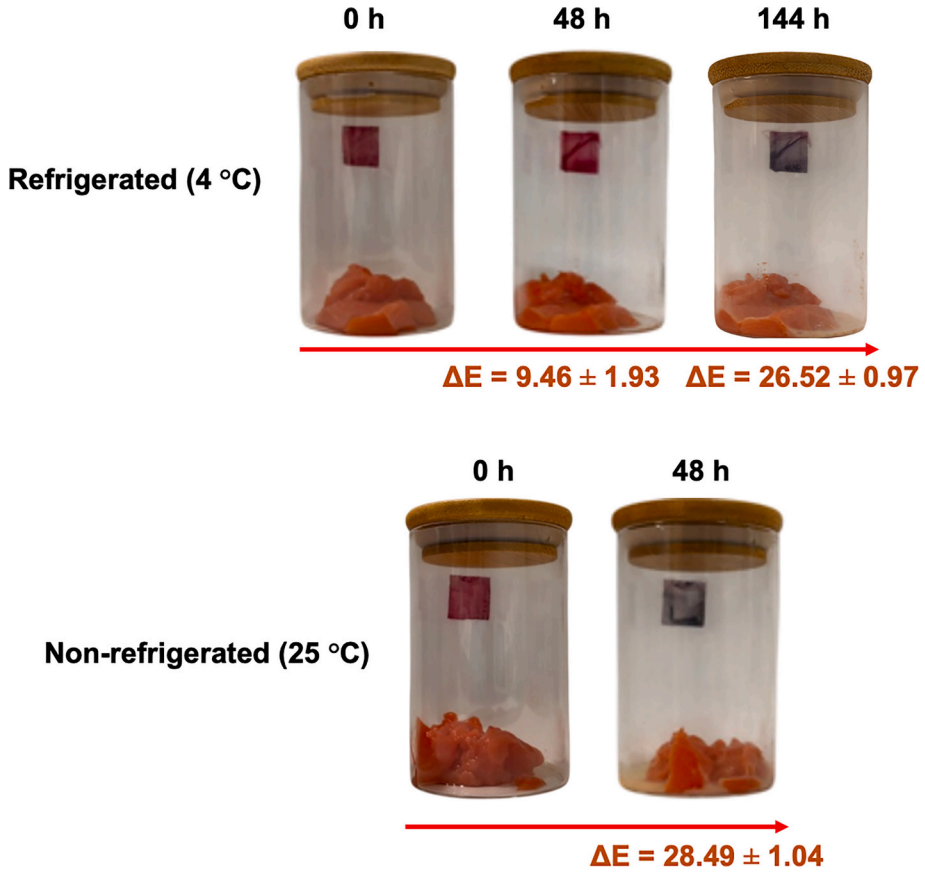

Fig. 5. Digital images of sealed transparent containers (250 mL) containing raw salmon samples (~20 g) and CA/BC colorimetric sensors (4 cm^2), during storage under refrigerated (4 °C) non-refrigerated (25 °C) conditions at selected time points.

values highlight the potential of the proposed colorimetric system as a practical freshness indicator for protein-rich foods.

4. Conclusion

We successfully fabricated cellulose acetate nanofibers functionalized with natural anthocyanins from grape pomace, sweet potatoes, and black carrots, with incorporation facilitated by pectin-NADES systems. Cellulose acetate nanofibrous mats were produced by solution blow spinning technique (SBS), using PEO as accessory polymer, which was removed after spinning (without affecting the final properties of the fibrous mats). Anthocyanins were incorporated onto the nanofibers surface by immersion, strategically modifying it to enhance the natural pigments' availability for sensing applications. The halochromic sensors exhibited suitable morphological, thermal, and water-related properties, while preserving the pH-dependent colorimetric behavior of anthocyanins. Black carrot anthocyanins, due to their higher pigment content and color strength, resulted in the most sensitive response, highlighting their potential as freshness indicators. The combination of SBS and NADES proved to be an efficient and sustainable strategy for producing intelligent nanofibers with prompt and stable visual responses to nitrogen-based analytes related to food spoilage conditions. A proof-of-concept assay using raw salmon packaging further demonstrated that the developed sensor was capable of qualitatively discriminating spoilage progression under different storage conditions based solely on headspace exposure, reinforcing its potential applicability as freshness indicators for protein-rich foods. Future studies should address response kinetics, humidity interference, long-term stability under light and thermal exposure, and sensor reversibility. In general, the results achieved in this study contribute to advancing eco-friendly solutions for intelligent packaging aimed at reducing food waste.

CRediT authorship contribution statement

Mirella Romanelli Vicente Bertolo-Cagnoto: Writing – review & editing, Writing – original draft, Methodology, Investigation, Formal analysis, Conceptualization. **Augusto Duarte Alvarenga:** Writing – original draft, Methodology, Investigation, Formal analysis. **Laís Angelice de Camargo:** Methodology, Investigation, Formal analysis. **Kelcilene Bruna Teodoro Costa:** Writing – original draft, Methodology, Investigation, Formal analysis. **Daniel Souza Correa:** Writing – review & editing, Supervision, Project administration.

Declaration of competing interest

The authors declare that they have no known competing financial interests or personal relationships that could have appeared to influence the work reported in this paper.

Acknowledgements

The authors thank the financial support from São Paulo Research Foundation (FAPESP) (Project numbers: 2023/06432-1, 2023/13428-0, 2018/22214-6, 2024/03972-8), Coordenação de Aperfeiçoamento de Pessoal de Nível Superior - Brasil (CAPES) - Código de Financiamento 001, and Conselho Nacional de Desenvolvimento Científico e Tecnológico (CNPq) (Project number: 351241/2023-0). The authors also thank Oterra® (Hørsholm, Denmark) for kindly providing the anthocyanins used in this study.

Appendix A. Supplementary data

Supplementary data to this article can be found online at https://doi.org/10.1016/j.ijbiomac.2026.151192.

Data availability

Data will be made available on request.

References

[1] A. Kramar, T. Luxbacher, N.M. Far, J. González-Benito, Active cellulose acetate/chitosan composite films prepared using solution blow spinning, Polymers 15 (2023) 3276, https://doi.org/10.3390/polym15153276.
[2] P.A.V. Freitas, N.S. Junior, R.R.A. Silva, et al., Intelligent cellulose acetate films using red cabbage extract for volatile base detection, LWT 132 (2020) 109780, https://doi.org/10.1016/j.lwt.2020.109780.
[3] H.M.C. Azeredo, D.S. Correa, Smart choices: mechanisms of intelligent food packaging, Curr. Res. Food Sci. 4 (2021) 932–936, https://doi.org/10.1016/j.crfs.2021.11.016.
[4] S. Siciliano, C.G. Lopresto, F. Lamonaca, Smart bio-packaging for food safety, Euro-Mediterr. J. Environ. Integr. 9 (13) (2024), https://doi.org/10.1007/s41207-024-00627-8.
[5] T. Zhang, H. Wang, D. Qi, L. Xia, L. Li, X. Li, S. Jiang, Multifunctional colorimetric cellulose acetate membrane with Perilla frutescens anthocyanins, Carbohydr. Polym. 278 (2022) 118914, https://doi.org/10.1016/j.carbpol.2021.118914.
[6] M.C. Silva-Pereira, J.A. Teixeira, V.A. Pereira-Júnior, R. Stefani, Chitosan/corn starch blend films with extract from Brassica oleracea (red cabbage) as a visual indicator of fish deterioration, LWT 61 (2015) 258–262, https://doi.org/10.1016/j.lwt.2014.11.041.
[7] R.S. Andre, M.H.M. Facure, L.A. Mercante, D.S. Correa, Electronic nose based on hybrid free-standing nanofibrous mats for meat spoilage monitoring, Sens. Actuator B-Chem. 353 (2022) 131114, https://doi.org/10.1016/j.snb.2021.131114.
[8] M. Schirone, L. Esposito, F. D'Onofrio, et al., Biogenic amines in meat and meat products, Foods 11 (6) (2022) 788, https://doi.org/10.3390/foods11060788.
[9] G.F. Nogueira, B.B. Meneghetti, I.H.B.T. Soares, et al., Arrowroot starch films with grape pomace anthocyanins, Int. J. Biol. Macromol. 265 (1) (2024) 130934, https://doi.org/10.1016/j.ijbiomac.2024.130934.
[10] Z. Zhou, D. Yang, Economical and eco-friendly isolation of anthocyanins from grape pomace, Food Chem. X 15 (2022) 100419, https://doi.org/10.1016/j.fochx.2022.100419.
[11] A. Saini, R. Hamid, R. Shams, K.K. Dash, A.M. Shaikh, B. Kovács, Anthocyanin extraction from black carrot, J. Agric. Food Res. 19 (2025) 101533, https://doi.org/10.1016/j.jafr.2024.101533.
[12] A. Li, R. Xiao, S. He, et al., Purple sweet potato anthocyanins: advances and applications, Molecules 24 (21) (2019) 3816, https://doi.org/10.3390/molecules24213816.
[13] C. Shen, Y. Cao, J. Rao, et al., Natamycin-loaded nanofibers by solution blow spinning, Food Packag. Shelf Life 29 (2021) 100721, https://doi.org/10.1016/j.fpsl.2021.100721.
[14] M.A.V. Rodrigues, M.R.V. Bertolo, M.M. Horn, A.B. Lugão, L.H.C. Mattoso, A.M. G. Plepis, Comparing solution blow spinning and electrospinning methods to produce collagen and gelatin ultrathin fibers: a review, Int. J. Biol. Macromol. 257 (2024) 125601, https://doi.org/10.1016/j.ijbiomac.2024.125601.
[15] K. Harini, M. Sukumar, Development of cellulose-based active packaging films, Carbohydr. Polym. 204 (2019) 202–213, https://doi.org/10.1016/j.carbpol.2018.10.018.
[16] M.R.V. Bertolo, S. Bogusz Junior, A.E. Mitchell, Green strategies for recovery of bioactive phenolic compounds from agro-industrial wastes using natural deep eutectic solvents, ACS Food Sci. Technol. 3 (12) (2023) 2144–2156, https://doi.org/10.1021/acsfoodscitech.3c00367.
[17] M.S. Jovanovic, N. Krgovic, J. Zivkovic, T. Stevic, G. Zdunic, D. Bigovic, K. Savikin, Ultrasound-assisted natural deep eutectic solvents extraction of bilberry anthocyanins, Plants 11 (2022) 2680, https://doi.org/10.3390/plants11202680.
[18] R. Thakur, V. Gupta, T. Ghosh, A.B. Das, Effect of anthocyanin–natural deep eutectic solvent (lactic acid/fructose) on mechanical, thermal, barrier, and pH-sensitive properties of polyvinyl alcohol-based edible films, Food Packag. Shelf Life 33 (2022) 100914, https://doi.org/10.1016/j.fpsl.2022.100914.
[19] M.A. Iqbal, S. Gohar, C. Zhu, G. Mayakrishnan, I.S. Kim, Green extract surface-coated electrospun cellulose nanofibers as an efficient, reversible, and reusable smart colorimetric sensor for real-time monitoring of chicken freshness, Curr. Res. Biotechnol. 6 (2024) 100192, https://doi.org/10.1016/j.crbiot.2024.100192.
[20] M.A. Iqbal, S. Gohar, C. Zhu, G. Mayakrishnan, I.S. Kim, Eggshell membrane as a novel and green platform for the preparation of highly efficient and reversible curcumin-based colorimetric sensor for monitoring chicken freshness, Int. J. Biol. Macromol. 266 (2024) 131089, https://doi.org/10.1016/j.ijbiomac.2024.131089.
[21] M.A. Iqbal, S. Gohar, M.S. Miah, R. Minami, J. Xiong, M.N. Sarwar, G. Mayakrishnan, I.S. Kim, Green, sustainable, and eco-friendly smart halochromic mats for food freshness detection, Mater. Today Sustain. (2025) 101125, https://doi.org/10.1016/j.mtsust.2025.101125.
[22] J. Lee, R.W. Durst, R.E. Wrolstad, et al., Determination of total monomeric anthocyanin pigment content by the pH differential method, J. AOAC Int. 88 (5) (2005) 1269–1278, https://doi.org/10.1093/jaoac/88.5.1269.
[23] M.R.V. Bertolo, L.F.R. Oliveira, G.M. Titato, F.M. Lanças, D.S. Correa, Sustainable extraction of value-added compounds from orange waste using natural deep eutectic solvents, J. Mol. Liq. 431 (2025) 127703, https://doi.org/10.1016/j.molliq.2025.127703.

[24] D. Yun, Y. He, H. Zhu, Y. Hui, C. Li, D. Chen, J. Liu, Smart packaging films based on locust bean gum and anthocyanin extracts, Int. J. Biol. Macromol. 205 (2022) 141–153, https://doi.org/10.1016/j.ijbiomac.2022.02.068.
[25] Q.N. Sultana, S. Absar, S. Hulsey, H. Schanz, M.R. Khan, Synthesis and processing of solution spun cellulose acetate fibers reinforced with carbon nanotubes, Proc. ASME Int. Mech. Eng. Congr. Expo. IMECE2015 (2015), https://doi.org/10.1115/IMECE2015-50804. V009T12A070.
[26] I. Chentir, C. Aribi, A.F. Tarchoun, H. Kchaou, M. Lamri, M. Nasri, D. Trache, Development of functional active films from gelatin/orange pomace pectin blends, Packag. Technol. Sci. 37 (1) (2024) 17–37, https://doi.org/10.1002/pts.2776.
[27] N. Wells, D. Yusufu, A. Mills, Colourimetric plastic film indicator for detection of volatile basic nitrogen compounds associated with fish spoilage, Talanta 194 (2019) 830–836, https://doi.org/10.1016/j.talanta.2018.11.020.
[28] M. Sohany, I.S.M.A. Tawakkal, S.H. Ariffin, N.N.A.K. Shah, Y.A. Yusof, Characterization of anthocyanin associated purple sweet potato starch and peel-based pH indicator films, Foods 10 (2021) 2005, https://doi.org/10.3390/foods10092005.
[29] S. Kamiloglu, A.A. Pasli, B. Ozcelik, J. Van Camp, E. Capanoglu, Colour retention and anthocyanin stability in black carrot products, J. Funct. Foods 13 (2015) 1–10, https://doi.org/10.1016/j.jff.2014.12.021.
[30] B.B. Yılmaz, N. Türker, pH and thermal stability of black carrot anthocyanins: impact of copigmentation, J. Food Meas. Charact. 18 (2024) 1499–1516, https://doi.org/10.1007/s11694-023-02230-x.
[31] J. Li, D. Zhao, M.A. Akram, et al., Environmental effects on anthocyanin accumulation in Lycium ruthenicum, J. Plant Physiol. 279 (2022) 153828, https://doi.org/10.1016/j.jplph.2022.153828.
[32] E. Anandhi, R. Shams, K.K. Dash, J.K. Bhasin, V.K. Pandey, A. Tripathi, Extraction and food enrichment applications of black carrot phytocompounds: a review, Appl. Food Res. 4 (1) (2024) 100420, https://doi.org/10.1016/j.afres.2024.100420.
[33] H. Xu, Y. Shi, L. Gao, N. Shi, J. Yang, R. Hao, Preparation and characterization of pH-responsive poly(vinyl alcohol)/chitosan/anthocyanin films, Food Sci. Technol. 43 (2023) e98022, https://doi.org/10.1590/fst.98022.
[34] D. Ji, Y. Lin, X. Guo, B. Ramasubramanian, R. Wang, N. Radacsi, R. Jose, X. Qin, S. Ramakrishna, Electrospinning of nanofibres, Nat. Rev. Methods Primers 4 (1) (2024), https://doi.org/10.1038/s43586-023-00278-z.
[35] E.J. Lee, H.S. Shin, Development of a freshness indicator for monitoring beef quality, Food Sci. Biotechnol. 28 (2019) 1899–1906, https://doi.org/10.1007/s10068-019-00633-5.
[36] H. Liu, C. Tang, Electrospinning of cellulose acetate in DMAc/acetone, Polym. J. 39 (1) (2007) 65–72, https://doi.org/10.1295/polymj.PJ2006117.
[37] M.E. Vallejos, M.S. Peresin, O.J. Rojas, All-cellulose composite fibers obtained by electrospinning dispersions of cellulose acetate and cellulose nanocrystals, J. Polym. Environ. 20 (4) (2012) 1075–1083, https://doi.org/10.1007/s10924-012-0499-1.
[38] K. Yan, Y. Le, H. Mengen, Z. Li, H. Zhulin, Effect of solution miscibility on morphology of coaxial electrospun cellulose acetate nanofibers, Polymers 13 (24) (2021), https://doi.org/10.3390/polym13244419.
[39] M.M.F. Ferrarezi, G.V. Rodrigues, M.I. Felisberti, M.D.C. Gonçalves, Investigation of cellulose acetate viscoelastic properties in different solvents, Eur. Polym. J. 49 (9) (2013) 2730–2737, https://doi.org/10.1016/j.eurpolymj.2013.06.007.
[40] I. Jilal, S. El Barkany, Z. Bahari, A. El Idrissi, A. Salhi, M. Abou-Salama, M. Ahari, H. Amhamdi, A new equation between surface tension and solubility parameters of cellulose derivatives depending on DS: application on cellulose acetate, Appl. J. Environ. Eng. Sci. 4 (2018).
[41] A.S. Buntjakov, V.M. Averyanova, Structure of solutions and films of cellulose acetate, J. Polym. Sci. C Polym. Symp. 38 (1972) 109–120, https://doi.org/10.1002/polc.5070380111.
[42] A. Kramar, J. González-Benito, Preparation of cellulose acetate film with dual hydrophobic–hydrophilic properties using solution blow spinning, Mater. Des. 227 (2023) 111788, https://doi.org/10.1016/j.matdes.2023.111788.
[43] M. Ahmadi Bonakdar, D. Rodrigue, Electrospinning: processes, structures, and materials, Macromol 4 (1) (2024) 58–103, https://doi.org/10.3390/macromol4010004.
[44] R.J. Souza, J.E. Soares Filho, T.A. Simões, J.E. Oliveira, E.S. Medeiros, Experimental investigation of solution blow spinning nozzle geometry and processing parameters on fiber morphology, ACS Appl. Polym. Mater. 6 (16) (2024), https://doi.org/10.1021/acsapm.4c01273.
[45] P.I.C. Claro, I. Cunha, R.T. Paschoalin, D. Gaspar, K. Miranda, O.N. Oliveira, R. Martins, L. Pereira, J.M. Marconcini, E. Fortunato, L.H.C. Mattoso, Ionic conductive cellulose mats by solution blow spinning for flexible electronics, ACS Appl. Mater. Interfaces 13 (22) (2021) 26237–26246, https://doi.org/10.1021/acsami.1c06274.
[46] A. Kramar, T. Luxbacher, J. González-Benito, Solution blow co-spinning of cellulose acetate with poly(ethylene oxide): structure, morphology and properties, Carbohydr. Polym. 320 (2023) 121225, https://doi.org/10.1016/j.carbpol.2023.121225.
[47] A. Verger, H. Kichou, N. Huang, X. Perse, I.M. Ardeza, C. Pradel, R.G.M. Conceicao, B. Atanasova, F.X. Legrand, A. Despres, L. Boudesocque-Delaye, E. Munnier, Effects of hydrophilic natural deep eutectic solvents on rheological, textural and sensory properties of carboxymethylcellulose-based hydrogels, ACS Sustain. Chem. Eng. 12 (18) (2024) 7187–7199, https://doi.org/10.1021/acssuschemeng.4c01866.
[48] E.J. Foster, R.J. Moon, U.P. Agarwal, et al., Current characterization methods for cellulose nanomaterials, Chem. Soc. Rev. 47 (8) (2018) 2609–2679, https://doi.org/10.1039/C6CS00895J.
[49] B.B. León-Vázquez, F. Rodríguez-Félix, W. Torres-Arreola, et al., Polylactic acid/cellulose acetate films incorporating black carrot extract, Int. J. Biol. Macromol. 317 (2025) 144840, https://doi.org/10.1016/j.ijbiomac.2025.144840.
[50] Z. Hong, W. Zhou, H. Deng, Q. Huang, Fabrication, performance and curcumin-controlled release of electrospun sarcoplasmic protein nanofiber films via layer-by-layer self-assembly, Colloids Surf. A Physicochem. Eng. Asp. 672 (2023) 131731, https://doi.org/10.1016/j.colsurfa.2023.131731.
[51] X. Xu, K. Huang, D. He, B. Huang, Q. Tang, H. Li, Z. Zhou, Biocompatible starch based smart active packaging film engineered with a novel CuNa-MOF colorimetric ammonia sensing agent based on crystal-to-crystal transformation, Food Packag. Shelf Life 49 (2025) 101498, https://doi.org/10.1016/j.fpsl.2025.101498.
[52] Z. Xu, Z. Cheng, Q. Tang, K. Huang, H. Li, Z. Zou, Ammonia-sensitive cellulose acetate-based films incorporated with co-BIT microcrystals for smart packaging application, Carbohydr. Polym. 316 (2023) 121045, https://doi.org/10.1016/j.carbpol.2023.121045.
[53] Q. Tang, Z. Zou, Y. Huang, S. Liang, H. Li, L. Xu, Novel ammonia-responsive carboxymethyl cellulose/co-MOF multifunctional films for real-time visual monitoring of seafood freshness, Int. J. Biol. Macromol. 230 (2023) 123129, https://doi.org/10.1016/j.ijbiomac.2023.123129.
[54] Y. Zhang, Q. Tang, K. Huang, Z. Xu, S. Feng, H. Li, Z. Zou, Developing strong and tough cellulose acetate/ZIF67 intelligent active films for shrimp freshness monitoring, Carbohydr. Polym. 302 (2023) 120375, https://doi.org/10.1016/j.carbpol.2022.120375.
[55] M. Brogly, S. Bistac, D. Bindel, Advanced surface FTIR spectroscopy analysis of poly(ethylene)-block-poly(ethylene oxide) thin film adsorbed on gold substrate, Appl. Surf. Sci. 603 (2022) 154428, https://doi.org/10.1016/j.apsusc.2022.154428.
[56] C. Bergeron, E. Perrier, A. Potier, G. Delmas, A study of the deformation, network, and aging of polyethylene oxide films by infrared spectroscopy and calorimetric measurements, Int. J. Spectrosc. (2012) 432046, https://doi.org/10.1155/2012/432046.
[57] M.A. Al-Akhras, M. Telfah, M.N. Shakhatreh, A. Telfah, M.S. Mousa, V. Narayanaswamy, I.M. Obaidat, Optical and chemical investigations of PEO thin films incorporated with curcumin nanoparticle: effect of film thickness, Biointerface Res. Appl. Chem. 13 (2) (2023) 143, https://doi.org/10.33263/BRIAC132.143.
[58] C. Voorhis, J. González-Benito, A. Kramar, "Nano in Nano"—incorporation of ZnO nanoparticles into cellulose acetate–poly(ethylene oxide) composite nanofibers using solution blow spinning, Polymers 16 (2024) 341, https://doi.org/10.3390/polym16030341.
[59] M. Liu, S. Zhang, Y. Ye, et al., Cellulose acetate@anthocyanin ultrafine fibers by electrospinning, Polymers 14 (19) (2022) 4036, https://doi.org/10.3390/polym14194036.
[60] A. Hamisu, A.M. Abubakar, K.S. Aminu, PEO-hBN-$NaClO_4$ polymer composite electrolyte for sodium ion batteries, Int. J. Sci. Basic Appl. Res. 45 (2) (2019) 104–117.
[61] H. Ayvaz, T. Cabaroglu, A. Akyildiz, C.U. Pala, R. Temizkan, E. Ağçam, Z. Ayvaz, A. Durazzo, M. Lucarini, R. Direito, Z. Diaconeasa, Anthocyanins: metabolic digestion, bioavailability, therapeutic effects, current pharmaceutical/industrial use, and innovation potential, Antioxidants 12 (1) (2023) 48, https://doi.org/10.3390/antiox12010048.
[62] B. Enaru, G. Drețcanu, T.D. Pop, A. Stănilă, Z. Diaconeasa, Anthocyanins: factors affecting their stability and degradation, Antioxidants 10 (12) (2021) 1967, https://doi.org/10.3390/antiox10121967.
[63] A. Patras, N.P. Brunton, C. O'Donnell, B.K. Tiwari, Thermal processing effects on anthocyanin stability, Trends Food Sci. Technol. 21 (1) (2010) 3–11, https://doi.org/10.1016/j.tifs.2009.07.004.
[64] K.M. Wani, R.V.S. Uppaluri, Characterization of pectin extracted from pomelo peel using ultrasound-assisted and hot water extraction, Appl. Food Res. 3 (7) (2023) 100345, https://doi.org/10.1016/j.afres.2023.100345.
[65] Z. Hong, W. Zhou, H. Deng, Q. Huang, Fabrication, performance and curcumin-controlled release of electrospun sarcoplasmic protein nanofiber films via layer-by-layer self-assembly, Colloids Surf. A Physicochem. Eng. Asp. 672 (2023) 131731, https://doi.org/10.1016/j.colsurfa.2023.131731.
[66] S. Majumder, A. Sharif, M.E. Hoque, Electrospun cellulose acetate nanofiber: Characterization and applications, in: Advanced Processing, Properties, and Applications of Starch and Other Bio-Based Polymers, Elsevier, 2020, pp. 225–252, https://doi.org/10.1016/B978-0-12-819661-8.00009-3.
[67] R. Erdmann, S. Kabasci, H.-P. Heim, Thermal properties of plasticized cellulose acetate and its β-relaxation phenomenon, Polymers 13 (9) (2021) 1356, https://doi.org/10.3390/polym13091356.
[68] T.F. Chen, C.T. Lo, Influence of interfacial compatibility on the crystallization behavior of electrospun core–sheath fibers, Polymer 283 (2023) 126200, https://doi.org/10.1016/j.polymer.2023.126200.
[69] S. Gopi, A. Pius, R. Kargl, K.S. Kleinschek, S. Thomas, Cellulose acetate/chitosan blend films as adsorbents, Polym. Bull. 76 (2019) 1557–1571, https://doi.org/10.1007/s00289-018-2467-y.
[70] A.W. Zykwinska, M.C.J. Ralet, C.D. Garnier, J.F.J. Thibault, Evidence for in vitro binding of pectin side chains to cellulose, Plant Physiol. 139 (1) (2005) 397–407, https://doi.org/10.1104/pp.105.065912.
[71] A. Petraru, S. Amariei, Edible packaging materials based on oilcakes, Polymers 15 (16) (2023) 3431, https://doi.org/10.3390/polym15163431.
[72] S.A. Minaker, R.H. Mason, D.R. Chow, Optimizing color performance of visualization systems, Ophthalmol. Sci. 1 (3) (2021) 100054, https://doi.org/10.1016/j.xops.2021.100054.

[73] P. You, L. Wang, N. Zhou, Y. Yang, J. Pang, pH-intelligent response fish packaging film based on konjac glucomannan/carboxymethyl cellulose/blackcurrant anthocyanin, Int. J. Biol. Macromol. 204 (2022) 386–396, https://doi.org/10.1016/j.ijbiomac.2022.02.027.
[74] Q. Ma, X. Lu, W. Wang, M.A. Hubbe, Y. Liu, J. Um, J. Wang, J. Sun, O.J. Rojas, Recent developments in colorimetric and optical indicators stimulated by volatile base nitrogen to monitor seafood freshness, Food Packag. Shelf Life 28 (2021) 100634, https://doi.org/10.1016/j.fpsl.2021.100634.
[75] H. Lee, M. Nishino, D. Sohn, J.S. Lee, I.S. Kim, Control of cellulose acetate nanofiber morphology via electrospinning, Cellulose 25 (5) (2018) 2829–2837, https://doi.org/10.1007/s10570-018-1744-0.